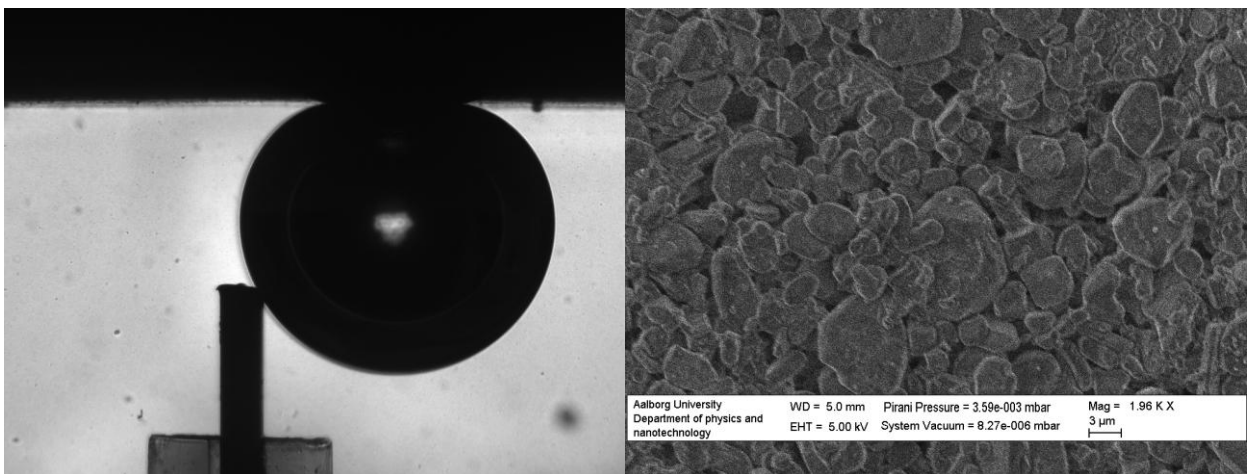


Thin anti-fouling film deposition on commercially available ceramic membrane filters



Lasse Christiansen

lassechristiansen88@gmail.com

Dennis Achton Nielsen

achtonium@gmail.com





**AALBORG UNIVERSITET** Institute of Physics and Nanotechnology  
 Skjernvej 4A  
 9220 Aalborg E  
 Phone: +45 9940 9215  
 Fax: +45 9940 9235  
<http://www.nano.aau.dk>

**Title:** Thin anti-fouling film deposition on commercially available ceramic membrane filters

**Theme:** Advanced applications of nanotechnology

**Project period**

Master thesis  
 September 2<sup>nd</sup> 2011 to May 31<sup>st</sup> 2012

**Project group**

5.219

**Participants**

Lasse Christiansen  
 Dennis Achton Nielsen

**Supervisor**

Leonid Gurevich -  
 (Associate professor,  
 Institute of Physics and Nanotechnology)  
 Peter Fojan -  
 (Associate professor,  
 Institute of Physics and Nanotechnology)

**Number printed:** 8

**Page count:** 77 doublepaged

**Complete:** May 31<sup>st</sup> 2012

**Synopsis:**

The main objective of this Master's thesis has been to add an anti-fouling polymer film to a membrane filter surface.

Based on the criteria for resisting protein adsorption polyethylene glycol (PEG) was chosen as anti-fouling material. Based on polymer chemistry and the work of Kahn et al. a surface initiated, anionic, ring-opening polymerisation of glycidol was chosen as polymerisation procedure.

The polymer growth procedure was initially tested on SiO<sub>2</sub> surfaces and was successfully transferred to sapphire substrates and ceramic membrane filter surfaces.

The anti-fouling properties were tested in dead-end protein filtration and simulated lake water filtration in a cross-flow setup. In both experimental series the addition of the PEG layer improved the anti-fouling properties of the treated filters compared to plain reference filters.



## Preface

This master's thesis is composed by project group NFM4 - 5.219c at the Institute of Physics and Nanotechnology at Aalborg university, in the period from September 1<sup>st</sup> 2011 to May 31<sup>st</sup> 2012 during the 9<sup>th</sup> and 10<sup>th</sup> semester. The project has been carried out in cooperation with Grundfos A/S. The target group of this project is students at a similar educational level and researchers dealing with fouling.

The main report consists of a theory chapter, a materials and methods chapter, and a chapter presenting the results. The theoretical chapter contains descriptions of flow and fouling of membrane filters, polymer chemistry, surface energy, and theory behind characterisation methods of the polymer film itself. The materials and methods chapter contains descriptions of the polymerisation process and descriptions of setups and procedures used to characterise the surface, the polymer film, and flow/fouling of treated and untreated filters.

References throughout the report are given as a number in a square bracket, where the number refers to a source given in the bibliography. If the reference is placed at the end of a section it refers to the whole section, however if it is placed elsewhere, it only refers to the specific statement, where it is located.

Finally we would like to use the opportunity to thank the people, who have helped us during our project. These are:

- **Allan Hjarbæk Holm** and **Karin Dooleweerd** from Grundfos A/S for providing materials, experimental setups and sparring during the project period.
- **Kasper Risgaard** for helping with the drop analysis setup and contact angle measurement software.
- **Pernille P. Davidsen** and **Susanne Ø. Lousdal** from Grundfos A/S for assistance with the flow tests carried out on Grundfos' test facilities.

II

## Signatures

---

Lasse Christiansen

Dennis Achton Nielsen

---

Date

# Contents

<b>1</b>	<b>Introduction</b>	<b>1</b>
1.1	Membrane bioreactors . . . . .	2
1.2	Ceramic filters . . . . .	4
1.3	Fouling . . . . .	5
1.4	Biofilms . . . . .	5
1.4.1	Build-up of biofilms . . . . .	6
1.5	Protein and bacterial adsorption . . . . .	7
1.6	Surface treatment . . . . .	8
1.7	Problem Statement . . . . .	10
<b>2</b>	<b>Theory</b>	<b>11</b>
2.1	Fouling impact on MBR performance . . . . .	11
2.2	Hydrophilicity and hydrophobicity . . . . .	16
2.2.1	Surface energy . . . . .	17
2.3	Polymerisation . . . . .	20
2.3.1	Ring opening polymerisation . . . . .	20
2.3.2	Hyperbranched polymerisation . . . . .	22
2.3.3	Polymerisation of glycidol on hydroxy-terminated surfaces. . . . .	22
2.4	Infra-red spectroscopy . . . . .	23
<b>3</b>	<b>Materials and methods</b>	<b>25</b>
3.1	Experimental procedure for polymerisation on substrates . . . . .	25
3.2	Ellipsometry . . . . .	26
3.3	Atomic force microscopy . . . . .	28
3.4	Fourier transform infrared spectroscopy . . . . .	29
3.5	Drop analysis . . . . .	30
3.6	Flow tests . . . . .	31
3.6.1	Dead end flow tests . . . . .	31
3.6.2	Cross-flow tests . . . . .	32
<b>4</b>	<b>Experiments and results</b>	<b>35</b>
4.1	Polymerisation on silicon substrates . . . . .	35

4.1.1	Ellipsometry . . . . .	35
4.1.2	AFM . . . . .	36
4.1.3	Results from polymerisation on silicon dioxide . . . . .	36
4.2	Polymerisation on aluminium oxide substrates . . . . .	37
4.2.1	Ellipsometry . . . . .	38
4.2.2	AFM measurements . . . . .	38
4.2.3	Infra-red spectroscopy . . . . .	38
4.2.4	Contact angle measurements . . . . .	42
4.3	Polymerisation on filters . . . . .	44
4.3.1	Drop analysis . . . . .	44
4.4	Hydrodynamic measurements . . . . .	46
4.4.1	Dead end flowtests . . . . .	46
4.4.2	Cross-flow tests . . . . .	52
<b>5</b>	<b>Discussion</b>	<b>57</b>
5.1	Silicon dioxide . . . . .	57
5.1.1	Results compared to Khan et al. . . . .	57
5.1.2	Process parameters . . . . .	57
5.1.3	Cleaning and possible problems . . . . .	58
5.1.4	Multi-wavelength ellipsometry and models for refractive indices . . . . .	58
5.2	Aluminium oxide . . . . .	58
5.2.1	Ellipsometry . . . . .	59
5.2.2	Infrared spectroscopy . . . . .	59
5.3	Drop analysis . . . . .	59
5.3.1	Aluminium oxide substrate . . . . .	59
5.3.2	Filters . . . . .	60
5.4	Filtration and flow . . . . .	61
5.4.1	Polymerisation on filters . . . . .	61
5.4.2	Dead-end filtration . . . . .	61
5.4.3	Cross-flow tests . . . . .	63
<b>6</b>	<b>Conclusion</b>	<b>65</b>
<b>7</b>	<b>Perspectives</b>	<b>67</b>
7.1	Future works . . . . .	67
7.2	Potential uses of the process . . . . .	68
<b>A</b>	<b>Laboratory safety</b>	<b>75</b>

# Chapter 1

## Introduction

Because of the constant increase in the world population and the demands for larger quantities of clean water, the task of supplying clean water becomes continuously harder. Therefore there is a demand for efficient water treatment in order to meet these demands, both for treating industrial wastewater, but also in order to supply sufficient volumes of drinking water. Progress has already been made, such as reverse osmosis (RO) technology and membrane bioreactors (MBR), but a lot of challenges still remain. RO and MBR plants are widely used in the industry in order to process their wastewater, before it can be discharged, but one target is also that eventually MBR technology can be implemented in plants that supply drinking water. MBR technology is a rapidly advancing field including both research and applications, but further development is necessary in order to reach even larger capacities. [1]

The research on MBR technology began over 35 years ago and has resulted in a number of MBR generations. Until now MBR installations are primarily used to treat industrial wastewater, but also municipal wastewater. However, it is expected that MBR technology will expand in treatment of municipal wastewater in the future, because of the advantages it presents, such as high effluent quality and low space requirements per throughput capacity. Full-scale industrial use of MBR installations dates back to the beginning of the 1990's in North America. Here they were only used in the industry, because the configuration of the MBR was unfavourable in municipal wastewater treatment, due to the high power consumption. In the mid 1990's a new MBR configuration was introduced, which allowed for expansion to use in municipal wastewater treatment. This also gave rise to an increasing research interest within this field, as can be seen in figure 1.1, where the number of peer-reviewed articles increased from around 15 in 1996 to 85 in 2004. [2]

Furthermore, among the research topics, membrane fouling has received a lot

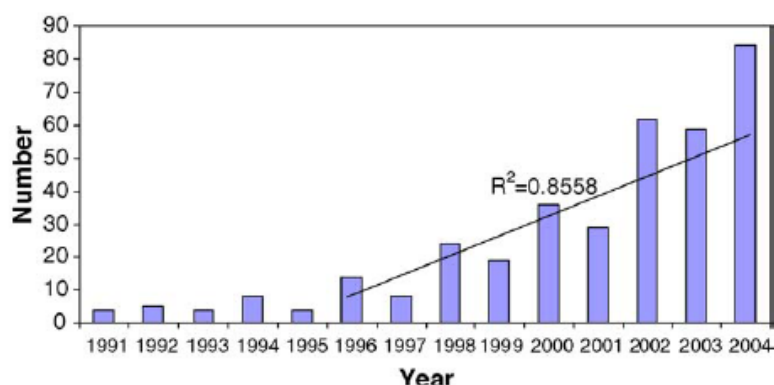


**Figure 1.1:** Number of peer-reviewed journal articles regarding the research in MBR technology. [2]

of attention, because this is one of the key performance limiting factors in an MBR. Earlier studies were concentrated around modelling and characterisation of membrane fouling. Recent studies are more focused on reducing membrane fouling with costs in mind. It is not enough to reduce membrane fouling, if the method is expensive compared to the savings in operation costs that is achieved through the anti-fouling modifications. [2]

One critical part in the MBR is a membrane filter that separates microorganisms and other organic material from the water. These filters are made with a wide range of pore sizes. They are subject to build-up of biological material when used. This reduces the flow through the membrane, because of the increase in hydraulic resistance caused by the blocking and narrowing of the pores and the build-up of a so-called cake-layer, which further increases the resistance and lowers the efficiency of the unit over time. This sets a limit to the efficiency at which an MBR plant can perform. For that reason fouling reduction is an interesting research area. Advances within this field would result in a higher throughput and a decrease in the need for chemical cleaning. This would allow the use of MBR technology to expand in domestic wastewater treatment, provided that a cost efficient solution can be found.

## 1.1 Membrane bioreactors

Membrane bioreactors are an advancing field in wastewater treatment. It has the advantage that a plant of MBR's in general takes up less space compared to ordinary municipal plants, which would be desirable in urban environments. They are capable of meeting very strict effluent quality requirements and can obtain the

same throughput as conventional water treatment plants around three times larger in size. This space efficiency both allows construction of new compact treatment plants as well as increasing the capacity of already existing plants. [3]

The MBR combines the process of activated sludge treatment and ultra/nano-filtration. In activated sludge treatment the water is led through a sludge containing microorganisms and enzymes that break down organic matter. This sludge is constantly aerated in order to keep the microorganisms alive. This process is, as mentioned combined with removal of organic matter by membrane filters. These filters are in most MBR's cleaned by pulsing jets of air on the filters from the side, which removes whatever is not adsorbed on the surface. However, all that is irreversibly adsorbed on the filters must be removed through chemical cleaning, which is a current disadvantage in MBR's. Therefore it is of interest to treat the membrane surfaces to make it less favourable for microorganisms to stick to the filter. [3]

One motivation for improving the operation time of membrane filters is that it will reduce the use of chemical cleaning agents on the filters. Furthermore it is preferable that the filtration system can operate for a long period of time without significant loss of efficiency due to fouling of the membranes. Membrane filtration is one of the key elements in the membrane bioreactor (MBR), such as used in the Grundfos BioBooster (GBB).

The GBB uses biological water treatment by using activated sludge and a mechanical treatment, where ultra filtration (UF) is used to physically separate biological and organic substances from the wastewater. In the BioBooster MBR concept the wastewater that enters the MBR is lead through active sludge and finally filtered through ceramic UF filters. Cross-flow impeller fans are inserted before the filtration part in order to reduce fouling by introducing a transverse velocity component. A GBB unit is shown in figure 1.2. [4]



**Figure 1.2:** Model of the Grundfos BioBooster MBR. The compartment to the left contains the activated sludge used to biologically treat the wastewater. Next there are cross flow impeller fans to reduce fouling, and to the right the filters are located. [4]

The filters in the GBB are, as any other surface in contact with water, subject to fouling, even though fouling is reduced by the cross-flow impellers. In this case fouling comes from the build-up of biofilm on the filters. This fouling reduces the efficiency of the GBB over time, because the flow through such a filter is reduced unless the trans-membrane pressure (TMP) is increased. Thereby it would

be favourable to apply an anti-fouling coating to the filters that would reduce the build-up of biofilm even more.

In many systems, a polymer filter would be easy to apply, and anti-fouling treatment could be done in several ways, due to the preparation process of a polymer filter. In MBR systems, like the GBB, the TMP makes a more durable membrane, like a ceramic membrane, more favourable.

## 1.2 Ceramic filters

Ceramics can be made in several different ways, and among the common are sintering and casting. Casting gives a strong, uniform, often crystalline body, which is of no interest with respect to filtration, while sintered ceramics are of more use.

A sintered object is formed by taking ceramic particles of a certain size distribution and pressing them together in the desired shape. This so-called green body is warmed up to 80-90 % of the absolute melting temperature of the material. This causes the particles to fuse at the edges, but without melting completely together. Various cavities are formed in between, and at lower temperatures these cavities will form networks, which may continue all the way through the body. [5]

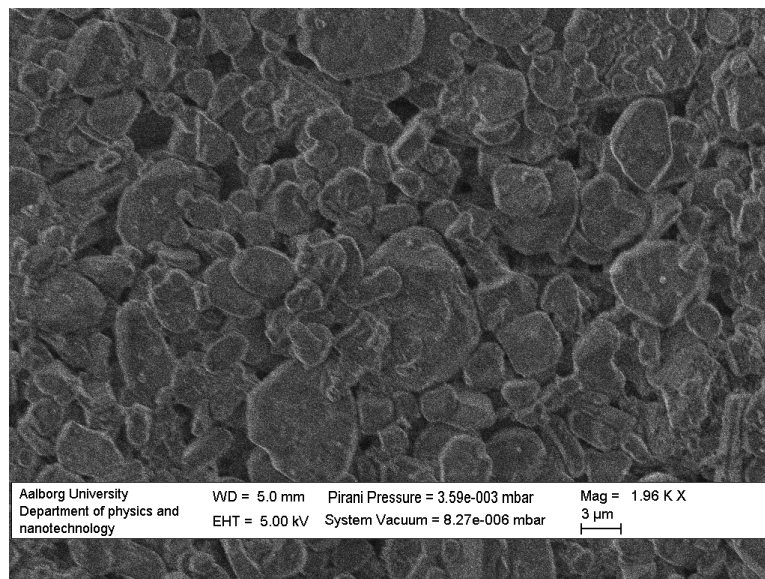


**Figure 1.3:** SEM image of a sintered aluminium oxide filter. According to the manufacturer this filter type should have an average pore diameter of 200 nm.

The pores can be used for filtration. Though they do not have a perfect circular shape, they are usually treated like they have. A flow analysis, called porometry, can be made, and by calculations the corresponding diameter of perfectly circular

pores to the flow of the filter is given. A SEM image of one of the filters used throughout this project is shown in figure 1.3. Here it is seen that there is a pore size distribution due to the arbitrary shape and size of the aluminium oxide particles.

### **1.3 Fouling**

Fouling refers to the accumulation of undesired material on surfaces, such as biofilms on membrane filters. This poses a great problem in ultra filtration processes of water in membrane bioreactors (MBR). Because of the increasing demand on water purity, the filtration and purification processes have become increasingly efficient. However, the need for membrane filters with pores small enough to separate microorganisms from the water has made the filtration process increasingly susceptible to fouling. Fouling thereby puts a restraint on the use of MBR technology, because it reduces the flow through the membrane filter and thereby reduces the efficiency of the MBR. [6]

Because of the impact of membrane fouling in MBR, much research have been done in order to both prevent and reduce fouling, but also to find methods for how it efficiently can be removed from the filter and pores. However, because of the many variables in such a problem, it is difficult to establish a model to describe the fouling process. Therefore it is more convenient to assess some of the properties of the system that largely affects the fouling process, such as the characteristics of the biological material in the water, membrane properties, and operating conditions in the MBR. These properties each affect the fouling process and can be assessed individually. [6]

Fouling can roughly be divided into two categories, reversible and irreversible fouling, even though the two types are not completely distinguishable. Reversible fouling refers to adsorption of biomass that is not yet chemically bound to the membrane and can be removed physically by for instance back-flush or cross-flow air pulsing. Irreversible fouling refers to adsorbed biomass that is chemically bound to the surface or in the pores and is removed chemically, by for instance chlorine. [6]

### **1.4 Biofilms**

A biofilm generally describes a cluster of microorganisms held together by extracellular slime that is excreted by the microorganisms. The slime consists of polymeric substances that form a web that holds the microorganisms in place and thereby immobilises them. Furthermore it is this extracellular polymeric substance that is responsible for sticking to a surface. A biofilm usually consists of several types of microorganisms that support each other, by sharing nutrients and waste.

[7]

The main criterion for the existence of a biofilm is basically that a surface is in contact with water. Even in high purity water environments microorganisms can survive in biofilms, because the slime efficiently captures and transports nutrients to the bacteria in the film. Furthermore biofilms can grow on smooth surfaces like polished steel, which means that it seems practically impossible to fully prevent the build-up of biofilm and therefore the focus is to optimise the operation time of a filter, rather than completely prevent fouling. In order to be able to modify the surface of the membrane one needs to know the mechanisms behind biofilm growth. [7]

### 1.4.1 Build-up of biofilms

The formation of biofilms is divided into individual steps that each contribute to the final biofilm. Initially, before the actual adhesion of cells, a layer of organic material, referred to as the surface conditioning layer, is deposited onto the surface. This can be proteins as well as other kinds of organic matter. This layer assists the adhesion of bacteria onto a surface, both because it roughens the surface, which makes it easier for microbial cells to attach to it, and it provides nutrients to the initially adhering bacteria. Furthermore this initial layer screens any surface charge that may prevent the adhesion of microorganisms. [7]

The next step is then the adhesion of the first bacteria, called pioneer bacteria. Initially, both temporary and permanent adhesion occurs, meaning that they either stick to the surface for some time and then desorb, or they irreversibly stick to the surface. Reversible adsorption is based on physical and electrostatic forces and is therefore characterised as physisorption. Physisorbed cells are not very strongly bound and can therefore desorb for instance due to shear from a flow. However, if the cells adhere to the surface for some time, they may be chemically and thereby irreversibly bound to the surface. [7]

During and after adsorption of the cells, these produce a web of extracellular polymeric substances (EPS), which mainly consist of polysaccharides. The EPS provides strong binding to the surface, but it also acts as a system that traps and transports nutrients from the water to the cells. This allows the cells to reproduce and thereby a colony of bacteria is obtained from the pioneer cells. The new cells also produce EPS, which highly increases the volume of the biofilm. A fully developed biofilm consists of 75-95% EPS. Besides acting as an adhering agent and nutrient provider, the EPS layer also protects the cells against antimicrobial biocides. This means that bacteria in a biofilm are harder to eliminate with for instance chlorine than free floating bacteria and proteins. Studies have shown that the production of EPS even may increase with the use of chlorine, making the film even more resistant against biocides. [7]

The EPS web may also capture other types of microbial cells and incorporate them in the biofilm by physically and electrically restraining them. These new bacteria may use the waste from other colonising bacteria as nutrients and vice versa and thereby a self supporting system can be obtained over time. The time it takes to develop a fully grown and functional biofilm may vary from hours to days or weeks, depending on the substrate surface properties as well as the aquatic environment. A biofilm may have a maximum film thickness that depends on the flow and environment. If the film grows into zones with fast and/or turbulent flow, parts of the film may be ripped off and transported with the flow. These environmental features define the maximum film thickness that can be maintained. [7]

As described biofilm exists practically where ever a surface is in contact with water, and thereby also on filters in filtration systems, which is undesirable. The build-up of biofilm onto a filter reduces the performance of filtration systems, because it lowers the flux through the filter and makes it necessary to frequently clean the filters or even replace them if the fouling is irreversible. Therefore in order to improve the process, build-up of the biofilm should be slowed down by for instance modifying the surface of the filters. Thereby the build-up is slowed down and the biofilm can be removed physically by back flush or cross flow, instead of chemical cleaning. [7]

## 1.5 Protein and bacterial adsorption

In order to further break down the biofilm formation process, it is of interest to investigate the compatibility of the individual components of the biofilm with a surface. One way to do that is to investigate the compatibility of different proteins to a given surface, because this gives a good impression of how well both the conditioning layer and pioneer bacteria adhere to a given surface. This is because the conditioning layer consists of proteins and other organic molecules and bacteria usually bind to a surface using their external pili, which are proteins.

As already established one key aspect in fouling of filters is the compatibility between foulant and the membrane filter surface. Therefore it is of interest to investigate the vast number of surface parameters that affect this compatibility. In this incomplete field of study researchers are searching for so-called inert surfaces, which are ideal surfaces to which proteins and bacteria do not adsorb. Proteins tend to adsorb irreversibly to surfaces and is therefore difficult to remove again. Whitesides et al. screened a vast number of different surfaces for their abilities to keep proteins from adsorbing irreversibly and found three key properties that were common for those of the surfaces that exhibited the inert surface quality. [8]

- The surface should contain hydrogen-bond donors and not hydrogen-bond acceptors.

- The surface should be charge neutral.
- The surface should be hydrophilic.

The exact explanation as to why these three properties are common for protein inert surfaces is not yet available, because of the complexity of the issue at hand. There are, however, some available explanations that support the results obtained by Whitesides et al.

First of all, the issue with hydrogen bonds can be explained by the general structure of proteins, which are chains of amino acids. Every link in this chain contains a N-H bond, which is a hydrogen bond donor. However, the amide is also a hydrogen bond acceptor and can for instance accept the hydrogen in an alcohol group, so it is far from the full explanation to the advantage of the first surface property.

The requirement of charge neutrality is due to minimisation of the electrostatic interaction between protein and surface. If the surface has a nonzero net charge it will give rise to an electrostatic attraction of the protein to the surface. This attraction is not an irreversible attraction, because the protein is not chemically bonded to the surface, but is considered physisorbed. Physisorbed species are physically bonded to the surface, but with a small release energy barrier. Still the electrostatic interaction enhances the possibility of irreversible attachment of the protein to the surface, because the physisorption increases the time in which the protein is in contact with the surface.

The effect of surface polarity to protein adsorption is not very understood. It is dependent on the side groups of the protein, because these can both be, charged, charge neutral, polar and non-polar. So the effect of hydrophilicity depends on the specific protein. However, for the attachment of bacterial and mammalian cells it makes sense that a hydrophilic surface is less favourable, because of the general hydrophobic nature of the cell walls.

## 1.6 Surface treatment

In order to decrease the fouling rate on these ceramic filters, some modifications of the filter surfaces can be made. The most obvious modification is to coat the filter surface with an anti-fouling layer. However, on filters with an average effective pore size of a few hundred nanometers the standard techniques, such as spin-, dip-, and spray-coating, are not useful, because these methods are likely to clog the pores since they do not restrict the polymer to the surface of the filter.

Different solutions could be found to this problem. One could be to use silane chemistry to deposit reacting groups on top of the filter, able to initiate polymerisations. This could for instance be an initiator for a Ziegler-Natta process, a surface

initiated atom transfer radical polymerisation or an anionic ring-opening polymerisation initiator. It could, of course, be favourable to avoid the step, where silane is deposited with plasma-CVD or other deposition techniques, if the initiator could react directly with the original surface. An issue with deposition of silicon is that it almost instantly will adsorb almost any particle it comes into contact with, due to its high polarisability. This means that any molecule with even a slightly inhomogeneous charge distribution will be physisorbed due to the mirror charge effect [9].

One solution to this problem is to grow the polymer layer directly on the filter surface by anionic ring-opening polymerisation. In order to initiate the polymerisation on the surface of a relatively inert material the surface must be activated. Kahn et al. [10] activated a  $\text{SiO}_2$  surface using a heated sodium methoxide solution in anhydrous methanol. Once the surface was activated they grew a branched PEG film by anionic ring-opening polymerisation at the surface. This technique could be useful in order to coat ceramic membrane filter surfaces, because the polymerisation is restricted to the surface. Thereby the filters will not clog provided that the thickness of the polymer layer can be controlled and kept small compared to the pore diameter.

The optimum choice of polymer depends on a number of factors. First of all it is preferred that the polymer surface is hydrophilic, because it is water that is to be transported through the filter and that the organic matter is mostly hydrophobic. Again one choice could be PEG, because of the high concentration of alcohol- and ether groups. Also the polymer should be quite durable so that the layer is not partly or completely removed, when the filter is used in an MBR. Hyperbranched PEG, as produced by Kahn et al., is chemically and mechanically robust, but in order to strengthen the polymer layer further, cross-linking of the branches can be introduced.

According to the common anti-fouling properties listed in section 1.5 a hyperbranched PEG layer is an obvious choice, because it meets the necessary properties characterising inert surfaces. The surface contains a high concentration of hydrogen bond donors in the form of alcohols terminating the PEG branches. It does contain hydrogen bond acceptors in the form of ether bonds, but these are not accessible because they are mostly screened by the alcohol terminations. The polymer is also hydrophilic and charge neutral, which meets the inert surface requirements. Though, it should be mentioned that PEG, as a polyether, can be oxidised by acids, and therefore its use is not recommended in very acidic environments.

In addition, unbranched PEG is used as an anti-fouling layer on silicon based bio-sensors, where it is critical that biological matter is not deposited onto the silicon biochip. [11]

## 1.7 Problem Statement

Filtration of liquids is done for several reasons, but in general unwished substances are removed, separated from the liquid by a membrane. These membranes will experience a deposition of waste on top of them, reducing the flux over time. In some cases this process is to some extent reversible, but the degree of reversibility will depend on the compatibility between the membrane and foulant.

A way to overcome this problem, and make the fouling more reversible could be to treat the surface in various ways. One approach could be to change the hydrophilicity of the surface. This could be done by adding a polymer layer on top of a ceramic membrane surface.

In this project there are two main goals. The first goal is to grow a thin anti-fouling film on the surface of a commercially available, sintered, ceramic membrane filter, without significant loss of permeability of the filter. The polymer film must be chemically bonded to the surface and durable enough to withstand long time use. This process should furthermore be reproducible, because one perspective of this project would be to implement this procedure in large scale production.

The second goal is to investigate the anti-fouling properties of this thin polymer film. This will concern the actual fouling process, where the goal is to slow down the flux decline by making the surface less compatible with the foulants. It will also concern the reversibility of foulant adsorption on the filter surface, where the goal is to enhance the ability to remove as much foulant as possible without the use of chemical cleaning agents.

## Chapter 2

# Theory

*This chapter contains the theoretical considerations necessary in order to treat membrane surfaces and characterise them. Initially MBR performance and fouling will be introduced. Next surface energy will be viewed, because changing the surface energy may be one method within anti-fouling measures. Then polymer chemistry and surface initiated ring-opening polymerisation is described in order to achieve a method to treat the membrane filters without clogging the pores. Finally, different characterisation methods able to provide knowledge of the grown polymer film will be discussed.*

### 2.1 Fouling impact on MBR performance

Membrane fouling in MBR systems is a result of the interaction between the membrane filter and the wastewater and activated sludge. It is thereby a process containing a vast number of variables and hence is difficult to model properly. Even though many models and experiments have been conducted in order to characterise the fouling impact on the flux through filters, these individual models only apply for a specific sludge composition and wastewater content. Because of the complexity of the overall problem no unified model exists yet. The general property that is to be determined is the total hydraulic resistance,  $R_t$ , of the membrane filter and how it develops over time, because the flux,  $J$ , is determined through the resistance by

$$J = \frac{TMP}{\eta R_t}, \quad (2.1)$$

where  $TMP$  is the trans-membrane pressure and  $\eta$  is the viscosity of the permeate. [6]

The task is to model, how the flow rate develops over time, which is a difficult task. One of the simpler models is the resistance-in-series model, where the total resistance is split into a sum of resistances covering individual steps of the fouling process and the initial resistance of the clean membrane filter. These resistances cover the resistance of the cake layer (reversible fouling) and the resistance of pore blocking and pore narrowing (irreversible fouling). However, the partition of the total resistance in this manner is questionable, because it assumes that the individual fouling processes are mutually independent, which might not be valid. Therefore the resistance  $R_t$  is often mentioned as a sum of the clean membrane resistance and the extra resistance from the total fouling. [6]

An often used way of modelling flux decline due to fouling is achieved by looking at individual fouling types in the fouling process and investigate their contributions to the flux decline individually. The fouling process is divided into four types, which are illustrated in figure 2.1.

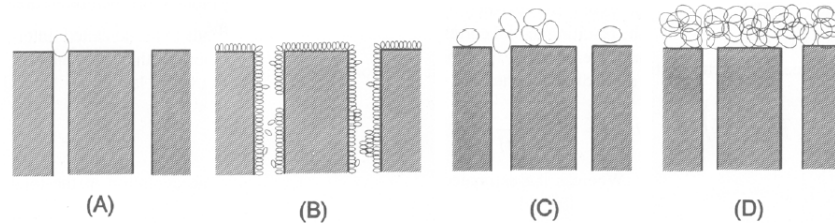


**Figure 2.1:** Schematic of the individual types in the fouling process. (A) Complete blocking, (B) standard blocking, (C) intermediate blocking, and (D) cake layer filtration. [12]

The individual steps of the fouling process are

- **Complete blocking** - Every particle arriving at the membrane blocks one or more pores without particle superposition.
- **Standard blocking** - Particle deposition on pore walls resulting in pore narrowing.
- **Intermediate blocking** - Arriving particles can either block a pore, attach to another pore-blocking particle or simply be adsorbed on the membrane surface.
- **Cake layer filtration** - A layer of particles on top of the membrane acts like an additional filter.

Each of these four fouling types are characterised by different types of flux decline, describing how the flux develops over time. These individual flux equations

mainly depend on the initial flux (flux through a clean membrane), the membrane properties, and fouling characteristics. With the different flux equations obtained the characteristic equation for the flux can be derived. The characteristic equation describes the second derivative of the time  $t$  with respect to the total permeate volume  $V$ . It is an often used method to describe a flux decline due to fouling, because it can be shown that all four fouling steps can be described by

$$\frac{d^2t}{dV^2} = \alpha \left( \frac{dt}{dV} \right)^\beta, \quad (2.2)$$

where  $\alpha$  and  $\beta$  are determined by analysis of each step in the fouling process. [12]

In the case of complete blocking it is assumed that every particle arriving at the membrane will block one or more pores, which implies that there is no superposition of particles in that process. The development of the flux over time in this step is given by an exponentially decaying function that starts with the initial flux  $J_0$  at the time  $t = 0$ . Therefore

$$J_V(t) = J_0 e^{-At}, \quad (2.3)$$

where  $A$  is the product of the initial velocity of the filtrate  $u_0$  and the membrane surface blocked per unit permeate volume  $K_A$ .

By integrating equation 2.3 one obtains a function for the permeate volume as a function of time, and by isolating the time in that expression a function for the time as a function of permeate volume. Finally the expression for the time function can be differentiated twice in order to get the characteristic equation.

$$\begin{aligned} V(t) &= \frac{J_0}{A} (1 - e^{-At}) \\ &\Downarrow \\ t(V) &= \frac{\ln \left( \frac{J_0}{J_0 - VA} \right)}{A} \\ &\Downarrow \\ \frac{d^2t}{dV^2} &= A \left( \frac{dt}{dV} \right)^2, \end{aligned} \quad (2.4)$$

meaning that for complete blocking  $\alpha = K_A u_0$  and  $\beta = 2$  [12].

In standard blocking it is assumed that every particle arriving to the filter is deposited internally on the pore walls and thereby decreasing the cross section area of the pores. Furthermore, it is assumed that the pores are cylindrical, which is also used as an assumption in capillary flow porometry. The volume flow rate through a cylindrical tube at constant pressure difference is proportional to the radius  $R$  to the power of four, which can be obtained by solving the Navier-Stokes equation for a cylinder [13]. This means that the flow rate scales with the reduction of the

area squared. The development of the flow rate over time is therefore given as

$$J_V(t) = \frac{J_0}{(1+Bt)^2}, \quad (2.5)$$

where  $B$  is the product of  $u_0$  and the decrease in pore cross section area per unit permeate volume  $K_B$ . The procedure to obtain the characteristic equation for is the same for complete blocking.

$$\begin{aligned} V(t) &= \frac{J_0 t}{1+Bt} \\ &\Downarrow \\ t(V) &= \frac{V}{J_0 - BV} \\ &\Downarrow \\ \left( \frac{d^2 t}{dV^2} \right) &= \frac{2B}{\sqrt{J_0}} \left( \frac{dt}{dV} \right)^{\frac{3}{2}}, \end{aligned} \quad (2.6)$$

meaning that  $\alpha = \frac{2K_B u_0}{\sqrt{J_0}}$  and  $\beta = \frac{3}{2}$  [12].

In intermediate blocking arriving particles will either completely block a pore or settle on an already blocking particle. Compared to complete blocking and standard blocking, that mainly occurs in the beginning of the fouling process, intermediate blocking usually occurs a bit later in the process, where pores already have been narrowed and blocked to some extent. Intermediate blocking can be seen as a part of the fouling process that is intermediate between pore blocking/narrowing and cake layer formation, which is the final step in the fouling process. Depending on the filter and foulant characteristics and flow rate, this step can be short in time and difficult to spot in flux measurements. However, the flux reduction over time for this step is modelled as

$$J_V(t) = \frac{J_0}{1+At}. \quad (2.7)$$

From equation 2.7 the total permeate volume and characteristic equation can be obtained:

$$\begin{aligned} V(t) &= \frac{J_0}{A} \ln(1+At) \\ &\Downarrow \\ t(V) &= \frac{1}{A} \left( e^{\frac{AV}{J_0}} - 1 \right) \\ &\Downarrow \\ \left( \frac{d^2 t}{dV^2} \right) &= \frac{A}{J_0} \left( \frac{dt}{dV} \right)^1. \end{aligned} \quad (2.8)$$

The final step in the fouling process is formation of the cake layer, which corresponds to adding an extra filter with a resistance  $R_C$ . The cake layer itself does

not block pores or cause pore narrowing, but simply builds up on top of the filter and thereby increases the total hydraulic resistance of the filter. When dealing with fouling of filters and anti-fouling approaches, one aim is to make the cake layer formation dominant over complete blocking and standard blocking, because the cake layer is easier to remove physically by back-flushing or cross-flow. Naturally it would be more preferable to completely avoid fouling, but in for instance dead end filtration, the foulants will somehow accumulate on the filter. If the filter can be modified so that it is unfavourable for the foulants to be in contact with the surface, it will be even less favourable to be inside a pore or blocking a pore, because of the greater contact area between membrane and foulant. The flux reduction due to cake layer build-up is

$$J_V(t) = \frac{J_0}{\sqrt{1+Ct}}, \quad (2.9)$$

where  $C = 2R_r K_C u_0$  with  $1/K_C$  being the total permeate volume per unit membrane area and  $R_r$  being the cake layer resistance relative to the resistance of a clean membrane. [12]

$$\begin{aligned} V(t) &= \frac{2J_0}{C} (\sqrt{1+Ct} - 1) \\ &\Downarrow \\ t(V) &= \frac{V^2 C}{4J_0^2} + \frac{V}{J} \\ &\Downarrow \\ \left( \frac{d^2 t}{dV^2} \right) &= \frac{C}{2J_0^2} \left( \frac{dt}{dV} \right)^0. \end{aligned} \quad (2.10)$$

The characteristic equation seen in 2.10 is interesting in the sense that it is represented by a horizontal line in a double logarithmic plot. Thereby it is easy to distinguish from the other fouling steps when plotting the characteristic equation. The characteristic equation coefficients are listed in table 2.1.

Fouling step	$\alpha$	$\beta$
Complete blocking	$K_A u_0$	2
Standard blocking	$\frac{2K_B u_0}{\sqrt{J_0}}$	$\frac{3}{2}$
Intermediate blocking	$\frac{K_A u_0}{J_0}$	1
Cake layer filtration	$\frac{J_0}{R K_C u_0}$	0

**Table 2.1:** Expressions for fouling parameters  $\alpha$  and  $\beta$  according to the characteristic equation.

The advantage of the characteristic equation is that if experimental flow data are plotted as  $\frac{d^2t}{dV^2}$  as a function of  $\frac{dt}{dV}$  in a double logarithmic coordinate system the result will approximately be a straight line with slope  $\beta$ . Thereby it is possible to determine the fouling type from the slope of the plot of the characteristic equation and if there occurs a shift in the fouling type over time. [12]

## 2.2 Hydrophilicity and hydrophobicity

The interaction between the surface of the membrane filter and the organic matter in wastewater is of great importance, when dealing with membrane bioreactors. The more compatible the biological matter is with the membrane surface, the harder it will be to remove it again, which will prevent efficient operation of MBR's over time. Therefore it is of interest to treat the membranes in order to lower their compatibility with the substances from the wastewater. One way is to investigate and alter the hydrophilic/hydrophobic properties of the filter in order to make it less compatible with the microorganisms. This change in hydrophilicity, that arises when treating the membrane surfaces, can also be used to determine whether or not the surface treatment was successful.

Hydrophilic/phobic properties are named after the way a substance interacts with water - a hydrophilic substance loves water, a hydrophobic one fears it. This meaning is applied, so that a hydrophobic substance interacts less favourable with water than a hydrophilic one, for instance splits in two phases for liquids, or forms a smaller interface area with an increasing contact angle for a solid surface. A classical and widely used example is the shape of a drop of water on a solid surface. On a hydrophilic surface the water drop will spread out as much as possible, because it is energetically favourable for it to be in contact with the surface. However it will still maintain a spherical-like shape in its contact with air, because this interface gives rise to surface free energy and the sphere provides the lowest surface to volume ratio. On the other hand the water drop will keep a small contact area to a hydrophobic surface, and approach the shape of a whole sphere, because this provides the lowest surface to volume ratio. [14]

Physisorption on a surface is, among other things, determined of the hydrophilicity or -phobicity of substance and surface. These properties are a result of energy minimisation in a system, where the molecular interactions determine the configuration of the system. These interactions derive from the symmetry and composition of the molecules. The charge distribution over the molecule, or absence of these, makes some molecules polar and some non-polar. This distribution is determined from both the different kinds of atoms in the molecule as well as the symmetry. If two atoms with similar electronegativities bond, they will share the electrons evenly across the bond, but if two atoms with different electronegativity bonds, the most electronegative atom will attract the electrons in the bond more than the other

atom. [14]

The difference in electronegativity is not enough to determine if a molecule is polar or non-polar. If a carbon chain is saturated with fluorine, it will be no more polar than if it was saturated with hydrogen. To make a molecule polar an asymmetry must be present. This can be caused by different atoms or electron lone pairs. Even though water consists of an oxygen atom with two hydrogen atoms, it is polar due to the two electron lone pairs. On the other hand a  $\text{CO}_2$  molecule non-polar due to its symmetry as seen in figure 2.2.

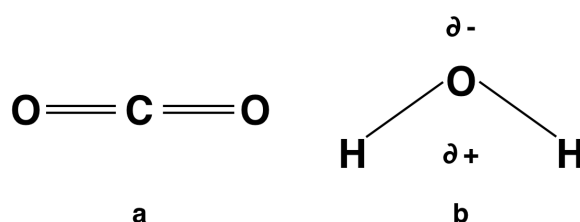


**Figure 2.2:** Example of polar and non-polar molecules.  $\text{CO}_2$  is non-polar because of its symmetry even though a single C-O bond is polar. On the other hand water is polar, because of the asymmetry caused by the two electron lone pairs.

When a molecule is polar, it will act as a dipole. This means that the most electropositive end will attract a more electronegative compound and vice versa. They will arrange in order to minimise the electrostatic energy of the system, and in this arrangement, the non-polar molecules will not be as favourable as a neighbour as a polar one. This leads to a separation, where polar molecules stick to polar, and non-polar to non-polar. The polar molecules will interact more strongly, for instance giving a great difference in the volatile properties of polar and non-polar molecules of similar size. [15]

Other properties than electronegativity and polarisation can also lead to different hydrophobic properties. According to Pomianowski and Grodzka [16], different, monocrystalline, pure metals without hydroxy groups, will arrange the first layer of water molecules on the surface differently, leading to different packings, with different contact angles and different surface energies.

### 2.2.1 Surface energy

Surface energy arises from the fact that at the surface there is a broken symmetry compared to an atom in the bulk, where all forces on that atom cancel each other out. At the surface, the resultant forces on the atoms are non-zero, because the surface atoms are not equally affected from the other atoms on the two sides of the interface. This difference in energy per contact area is known as the surface energy or surface tension. When energy is used to treat the conformation of a system,

energy minimisation is the governing principle. The lowest possible state is the most stable.

For a two-phase system, a gas and a liquid or a hydrophobic and a hydrophilic liquid for instance, the minimisation of energy will lead to a spherical droplet if the two parts are not fully mixable and gravity is negligible, again because the sphere gives the lowest surface to volume ratio and will minimise the surface energy. One phase might be partially dissolved in the other. This spherical form might also apply if a third substance, for instance a surface, is introduced, but in general this cannot be expected.

Instead a general equation can be introduced for a liquid drop on top of a horizontal solid surface. As in thermodynamics, a work function is introduced that describes the work in the triple point, where the three phases meet as seen in figure 2.3.

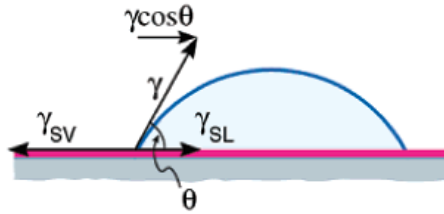


**Figure 2.3:** Forces on the triple point of a liquid drop on a solid surface. [14]

This work function will depend on the surface work and the volume work, and can be defined as

$$\delta w = \gamma_{12}dA_{12} + \gamma_{23}dA_{23} + \gamma_{13}dA_{13} + \Delta P dV \quad (2.11)$$

where  $\gamma_{12}$  is the surface energy between phase one and two, and  $A_{12}$  is the surface area shared between phase one and two. For a gas(G), liquid(L), solid surface(S) system, this results in an equation of the form

$$\delta w = \gamma_{GL}dA_{GL} + \gamma_{LS}dA_{LS} + \gamma_{GS}dA_{GS} + \Delta P dV. \quad (2.12)$$

When this system is close to be in equilibrium, it is noted that the volume change of the liquid  $dV$ , can be approximated to zero. This is due to the fact that no compression of the liquid occurs. Furthermore usually a droplet in equilibrium is considered, meaning that the work in the triple point is zero. So setting  $dV$  and  $\delta W$  to zero, equation 2.12 can be reduced to the well-known Young's equation given by

$$\gamma_{SL} + \gamma_{GL} \cos(\theta_0) = \gamma_{GS}, \quad (2.13)$$

where  $\theta_0$  is Young's equilibrium contact angle [14].

This is the classical approach, but Rafael Tadmor also introduces the concept of line energy, which is the energy contribution from the line where all three phases are in contact. As shown, both theoretically and in practice, this line energy gives rise to an angle spectrum rather than providing a single equilibrium contact angle, since it tends to pin the edges of the drop at this line. It takes imperfections of the surface into account, and is proportional to the length of the line, leading to

$$\delta w = \gamma_{GL}dA_{GL} + \gamma_{LS}dA_{LS} + \gamma_{GS}dA_{GS} - kdL, \quad (2.14)$$

where the assumption of constant volume has been applied,  $k$  is the line energy per unit length and  $dL$  is the length increment going around the circle of triple points [14].

Since it is still assumed that the drop is in equilibrium,  $\delta w$  is again set to zero. It can be noted that the change in surface/liquid area only can happen on expense of surface/gas area, which means that

$$dA_{SL} = -dA_{SG}, \quad (2.15)$$

leading to

$$0 = \gamma_{GL}dA_{GL} + (\gamma_{LS} - \gamma_{GS})dA_{LS} + kdL. \quad (2.16)$$

It is noted that  $\gamma_{GL}$  usually is written as  $\gamma$ , which is the surface tension of the liquid. Furthermore  $\Delta\gamma = \gamma_{GS} - \gamma_{LS}$  is introduced to simplify the expression. Equation 2.16 can then be rearranged to

$$\gamma \frac{dA_{GL}}{dA_{LS}} - \Delta\gamma + k \frac{dL}{dA_{LS}} = 0. \quad (2.17)$$

It can be shown by geometry, under the assumption of constant volume, that

$$\frac{dA_{GL}}{dA_{LS}} = \cos(\theta) \quad (2.18)$$

where  $\theta$  is the actual contact angle between the surface and the droplet in the contact point. Moreover, Tadmor shows that

$$\frac{dL}{dA_{LS}} = \left( \frac{\pi 2 - 3\cos(\theta) + \cos^3(\theta)}{3 V \sin^3(\theta)} \right), \quad (2.19)$$

still under the assumption of constant droplet volume  $V$  [14].

Through the last three equations, and by noting that  $\cos(\theta_0) = \frac{\Delta\gamma}{\gamma}$  from Young's equation, an expression for the line energy  $k$  can be generated as

$$k = \Delta\gamma V^{\frac{1}{3}} \left( \frac{\cos(\theta)}{\cos(\theta_0)} - 1 \right) \left( \frac{3 \sin^3(\theta)}{\pi 2 - 3 \cos(\theta) + \cos^3(\theta)} \right), \quad (2.20)$$

which shows that the line energy depends on the equilibrium contact angle besides being a function of surface defects.

The line energy gives rise to an angle hysteresis rather than a fixed angle. However, fixed and isotropically distributed surface defects will give rise to a fixed maximum value of  $k$ , which then can provide a maximum and minimum angle of the actual angle interval. These are the advancing and receding angles, because the maximum contact angle is obtained as the drop is advancing, while the line energy tries to pin the drop edge on the line and the minimum angle is obtained, when the drop is receding. These scenarios correspond to the maximum value of the line energy and its negative value, since it is assumed, that the surface defects are isotropic in manner and distribution. [14]

This corresponds to setting  $k(\theta_A) = -k(\theta_R) =$  from which  $\theta_0$  as a function of  $\theta_A$  and  $\theta_R$  can be obtained as

$$\theta_0 = \cos^{-1} \left( \frac{\Gamma_A \cos(\theta_A) + \Gamma_R \cos(\theta_R)}{\Gamma_A + \Gamma_R} \right), \quad (2.21)$$

where

$$\Gamma_X = \left( \frac{\sin^3(\theta_X)}{2 - 3 \cos(\theta_X) + \cos^3(\theta_X)} \right)^{\frac{1}{3}}, \quad X = A, R. \quad (2.22)$$

Equations 2.21 and 2.22 are the main equations used in determining Young's equilibrium contact angle in practice and are of great importance when dealing with determining and detecting changes in surface properties. These two equations will also be used in this project when investigating the treated filters. The method of experimentally determining  $\theta_A$  and  $\theta_R$  through drop analysis will be explained in section 3.5.

## 2.3 Polymerisation

Hydrophilic properties of a surface can be changed by changing the composition of the surface. If, for instance a highly hydrophilic polymer layer can be coated onto a surface which is not as hydrophilic, it will adapt the properties of the polymer.

Polymers can be produced by numerous chemical processes, in general called polymerisation. These processes can be divided into different groups according to reaction mechanisms and products, like radical or anionic vinyl polymerisations, surface catalysed polymerisations like Ziegler-Natta, chain reactions and ring opening polymerisation.

### 2.3.1 Ring opening polymerisation

Ring opening polymerisation is the technique used in the polymerisation of the thin films in this project. Ring opening polymerisation occurs when a ring system in an

organic molecule (the monomer) is opened, joined with a series of already opened rings (the polymer), and then able to open a new ring. The most used in industry are lactams, cyclic siloxanes, and epoxides. Glycidol, used in this project, is an epoxide.

There are two general forms of polymerisation from ring structures, they can be seen in figures 2.4 and 2.5.

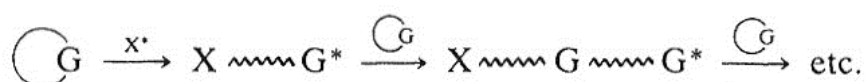


**Figure 2.4:** The monomer is attacked by the species  $X^*$  at the site of the functional group  $G$ . This causes a ring opening and leaves the group  $G^*$  with properties similar to  $X^*$  in respect of continuing the ring opening. [17]

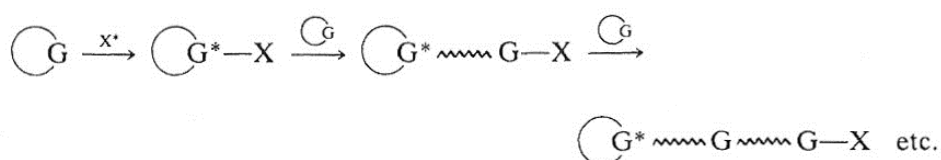


**Figure 2.5:** The monomer is attacked by  $X^*$  which couples to it. This functionalises the active group  $G$ , making it  $G^*$ , which is capable of opening the ring and when it undergoes reaction with a new monomer, it causes a new  $G^*$  to be created. [17]

In addition, the second model has a form, where an initiator, composed of two parts, becomes ending groups of the polymer, and the monomers are added in between. This can be seen on figure 2.6.

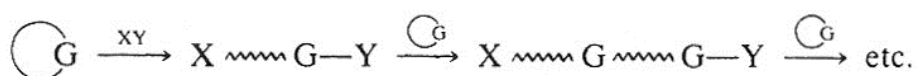


**Figure 2.6:** The monomer is attacked by the species  $XY$ , where  $X$  serves as a ring opener and  $Y$  then will link to the functional group,  $G$ . The  $G-Y$  group is then able to attack a new monomer, joining it to the chain and passing the  $Y$  to a new  $G$ . [17]

The most common types of ring opening polymerisation are ionic polymerisations and polymerisation with coordination compounds. Other molecule compounds can also be used, as for example water, alcohols or amines, but free radical polymerisations are less common in ring-opening polymerisation.

Different ring sizes have very different reactivities, among other things due to the different ring strains. The reactivity of the rings can be listed with respect to number of molecules in the ring as

$$3 > 4 > 8 > 7 > 5 > 6, \quad (2.23)$$

this is with respect to the same functional groups. [17]

### 2.3.2 Hyperbranched polymerisation

When the polymerisation of a chain polymer takes place an attacking group and a reacting group should be present, so the reactive group can be attacked and a chain be formed. If more than one of these groups are present in the polymer, a network can be formed instead of chains. This comes in two forms - cross-linking and hyperbranching. Cross-linking occurs in polymers that polymerises spontaneously like polyurethane, hyperbranching is found in polymer systems, where the attacking group for instance has to be activated by ionic polymerisation or free radical polymerisation. If a polymer with more than one possible attacking group, like glycidol, it has a possibility distribution that one of all the attacking groups is activated after a reaction. Hyperbranching will then occur like a weighted random walk, leading to a broccoli-like growth. [17]

### 2.3.3 Polymerisation of glycidol on hydroxy-terminated surfaces.

In this project a hyperbranched PEG film is grown on top of different hydroxy-terminated surfaces by using a two-step process. In order to begin polymerisation an initiator is needed and in this reaction an anion is to be used. The surface is activated by letting the surface react with a heated sodium methoxide solution in anhydrous methanol through the reaction



It must be anhydrous methanol, because water will react with sodium methoxide resulting in sodium hydroxide and methanol. This reaction must be avoided, because sodium hydroxide can not activate the surface.

With this reaction the surface obtains O-Na terminations, which is an ionic bond compared to the O-H termination. Thereby the oxygen atom can be characterised as a nucleophile and can attack electron poor sites. This is used to initiate the polymerisation process, which is an anionic ring-opening polymerisation process, corresponding to the one seen in figure 2.6. This process is also carried out at high temperatures, because this allows the sodium ion to substitute itself for a hydrogen atom in a new O-H termination, which allows the reaction to continue.

As the oxygen atom attacks the epoxy ring, the ring is opened and binds to the surface oxygen atom, which releases the sodium ion, which then is substituted to a new O-H termination.

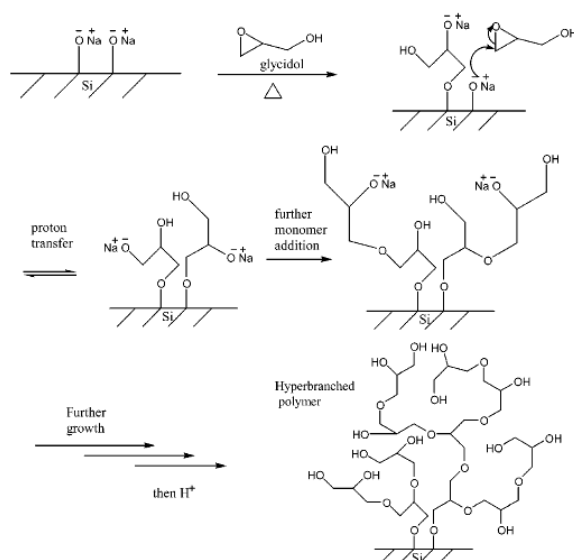


**Figure 2.7:** Polymerisation reaction of glycidol on O-Na terminated surface. [10]

The reason that this procedure results in a branched polymer is that when the epoxide is opened the unit contains two O-H terminations, which allows the reaction to run in two directions per monomer. The reaction is repeated until all the monomer is used, the reaction is stopped, or until the O-Na terminations is no longer accessible to the monomer. The reaction scheme for this particular polymerisation process is shown in figure 2.7. [10]

## 2.4 Infra-red spectroscopy

Infra-red (IR) spectroscopy is a method used to determine the presence of chemical structures in a gas, solution, liquid or solid. Radiation in the infra-red spectrum is used to excite vibrational states in molecules. By measuring the absorption unique fingerprints of different structures can be detected, because different bonds in the molecules are characterised by different vibrational excitation energies. The absorption bands are located in the wavelength intervals between 2500 nm and 25000 nm. This corresponds 0.05 eV to 0.50 eV in photon energies, or 400 cm<sup>-1</sup> to 4000 cm<sup>-1</sup> in the, for IR spectroscopy, often used wave number. The wave number is reciprocal wavelength. The general relation between these values is

$$E = h\nu = \frac{hc}{\lambda}, \quad (2.25)$$

where  $E$  is the energy,  $h$  is Planks constant,  $\nu$  is the frequency,  $c$  is the speed of light and  $\lambda$  is the wavelength. Each different vibrational state of the bonds in a molecule has an excitation energy, which can be calculated through quantum mechanics.

By observing the values of the absorbency with respect to the wavelength it can be seen where vibrational states are excited, and by comparing them to tables of absorption values the present bindings can be found. The expected peaks for PEG is found at 2960-2850  $\text{cm}^{-1}$  for C-H bonds, 3600-3200  $\text{cm}^{-1}$  for O-H bonds and 1150-1070  $\text{cm}^{-1}$  for the ether bond. If un-polymerised glycidol is present, the peak for the epoxide should be located at 3030-3050  $\text{cm}^{-1}$ . [18]

A measurement with infra-red spectroscopy is done by transilluminating a sample with infra-red radiation and measure the absorbency compared to a reference sample. The transparency to a given wavelength,  $D_\lambda$ , of the sample is given by

$$D_\lambda = \frac{I_\lambda}{I_{0\lambda}} \quad (2.26)$$

where  $I$  and  $I_0$  is the intensity after the transillumination of the sample and the reference respectively. The absorbency is then given by

$$E_\lambda = \log(1/D_\lambda) \quad (2.27)$$

## Chapter 3

# Materials and methods

*This chapter contains descriptions of the procedures of the different production and characterisation methods used throughout this project. First the polymerisation procedure is described for both silicon oxide and sapphire substrates as well as the filters. Next the ellipsometry procedure, including a model for the refractive index of PEG, is presented. Then the procedure for drop analysis and atomic force microscopy, used to determine surface hydrophilicity and roughness, is explained. Next the IR spectrometry procedure is viewed and finally the two types of flow tests used in this project are explained.*

### 3.1 Experimental procedure for polymerisation on substrates

In order to polymerise PEG on top of a substrate, an experimental procedure similar to the one of Khan et al. was designed. [10]

For silicon oxide, a thermal oxide is grown on pieces of silicon wafer (10x10mm) by heating them in an oven at 900°C in atmospheric air for 60 minutes to obtain a silicon oxide layer with a thickness around 50-100 nm. This thickness is measured by using ellipsometry. Only with respect to the oxide growth does the process differ from growing PEG on aluminium oxide. After this step the process is similar.

First the substrate is cleaned with ultrasound; two minutes in acetone, then two minutes in water followed by two minutes in ethanol. Then it is dried with nitrogen. Finally, it is cleaned in a UV cleaner for five minutes and transferred to clean water in order to increase the concentration of hydroxy-terminations on the surface.

During the project period two different setups were used. Initially, for poly-

merisation on silicon oxide substrates a "starfish" setup was used, where the reaction chambers were two-necked flasks with condensers on one neck and nitrogen flow inlets on the other. To the filters and sapphire substrate a simpler setup was used; a wide-necked bluecap bottle was lowered into an oil bath by which the reaction temperature was controlled.

The substrate is transferred to a reaction cell, which is placed in a fumehood due to the safety hazards of the chemicals used.

In order to activate the surface, the substrate is treated with a 0.18M sodium methoxide solution in anhydrous methanol at 75°C for an hour. The solution is removed afterwards and the substrate is washed twice with anhydrous methanol.

With the substrate in the bottom of the cell glycidol is added so it covers the entire substrate and the reaction cell is heated up. On the silicon oxide substrate three different temperatures are used, which are 110, 125, and 140°C, measured in the heat cap in the setup. In the other setup the temperature of the oil bath was kept at 110°C. The side of the substrate which should be coated has to face downwards toward the glycidol, so it is in contact all the time, because some substrates tend to float.

The system is left to polymerise for 60 minutes. After this the reactor is left to cool down until the remaining glycidol can be transferred safely to waste. Then the sample is cleaned with ethanol and water and dried with nitrogen gas. The thickness of the PEG layer can then be measured using ellipsometry.

## 3.2 Ellipsometry

Ellipsometry can be used to determine the thickness of a thin film on top of a substrate, if the refractive index of the film is known. It is also possible to fit the results to both thickness and refractive index and thereby establish an experimentally determined model for the refractive index of the polymer; however in the case of PEG on top of silicon dioxide this is not possible, because the refractive indices of silicon dioxide and PEG are quite similar.

In ellipsometry the film thickness of a material, with a known refractive index, is determined by directing a beam of linearly polarised light onto the surface and evaluating the reflected elliptically polarised light after reflection at the surface, as seen in figure 3.1. The measured data are then fitted to a theoretical output model of the film and substrate and thereby the thickness can be determined.

In this project oxide layers with thicknesses between 50 and 100 nm are grown thermally on silicon and afterwards the thicknesses of each sample are measured using ellipsometry. These thicknesses are important, because otherwise it is difficult to distinguish the PEG film from the oxide layer in the measurements, because of the similarity in their refractive indices.

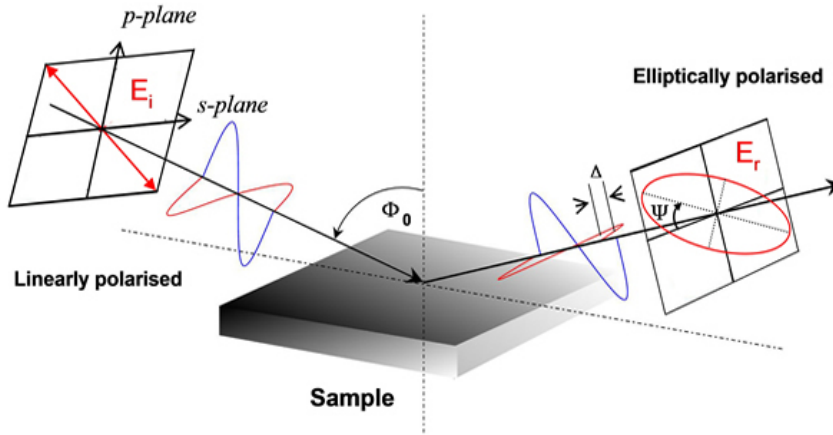


**Figure 3.1:** The process utilised in ellipsometry. Linearly polarised light is directed onto the sample and the reflected, elliptically polarised light is detected and analysed. [19]

Growing PEG on aluminium oxide has the advantage that no additional layer is present, so that the only variable is the PEG layer thickness. However, the aluminium oxide substrate is transparent, which causes that besides the signals from the air/PEG and PEG/aluminium oxide interfaces, there will also be a considerable signal from the bottom of the aluminium oxide substrate. This extra signal will disturb the measurement to such extent that no PEG thickness can be determined. In order to avoid signals reflected from the back of the samples the substrates must be polished into a wedge shape, which will cause the undesired signal to be directed away from the detector. This was done on silicon carbide, on a rotating polisher with first 300 grains pr. square centimeter, and afterwards 1200. In order to get an angled surface, a special surface mount was used, where the angle could be changed, and the sample lowered stepwise on to the silicon carbide mat.

In the ellipsometry software there are numerous models for the refractive index of silicon dioxide, and from these a Sellmeyer model has been chosen. Also several models for aluminium oxide are present, where a Tauc-Lorenz model for sapphire was chosen. However, there are no models of the refractive index of PEG to be used in the software, so that model must be defined otherwise. The refractive index of PEG also depends on the molecular weight of the polymer. In this project a Cauchy model, experimentally derived by [20], is used. They suggested Cauchy models for PEG with different molecular weights.

In the ellipsometer software the Cauchy model for refractive indices as a function of wavelength in nanometers is given by

$$n(\lambda) = n_0 + c_1 \frac{n_1}{\lambda^2} + c_2 \frac{n_2}{\lambda^4}, \quad (3.1)$$

where  $\lambda$  is the wavelength in nanometers,  $n_0$ ,  $n_1$ , and  $n_2$  are Cauchy coefficients

(usually determined experimentally) and  $c_1 = 10^2$  and  $c_2 = 10^7$  are multipliers introduced for convenience in the software. Compared to the results from [20] the Cauchy coefficients used in this work are  $n_0 = 1.4581$ ,  $n_1 = 39.41$ , and  $n_2 = 5.39$ , which are the coefficients of PEG with a molecular weight of 400. Moreover, it is assumed that PEG has a zero imaginary part of the refractive index, which might not be correct; however, for layers as thin as 5 nm it is a fair assumption that no light is absorbed in the polymer layer.

Since the thickness of the silicon dioxide is known and the refractive indices are modelled, the only remaining fitting parameter is the PEG film thickness, which can be estimated by fitting the output data to the theoretical model. On aluminium oxide the process is similarly straightforward again because the only unknown is the PEG layer thickness. One drawback is, however, that scattered light from the polished side of the substrate can still be detected as noise on the output.

One general drawback of this technique is that it outputs an average thickness. So theoretically a distribution of grown domains could output the same result as the thickness of a smooth layer and therefore investigation of the surface topography is also necessary.

### 3.3 Atomic force microscopy

In order to characterise the surface of the polymer, Atomic Force Microscopy (AFM) was used. This technique gives a surface topography, which is relevant for both the biocompatibility and the composition of the surface layer.

The probe is mounted on one end of a cantilever and has a tip curvature in the range of a few nanometers. When the probe is brought into proximity to the surface of the sample, the cantilever is deflected by the forces between the sample and the probe. The deflection is usually measured by directing a laser beam onto the cantilever and determine the surface topography by detecting the deflection of the laser beam, as can be seen in figure 3.2. This is done by the probe scanning a number of points per line and an equivalent number of lines per frame. The height is scanned in each of these points and thereby the surface topography is generated. Since each point has been given a height value, properties like surface roughness can easily be calculated. In practice the scanning is done by keeping the cantilever and probe fixed and moving the stage with the sample, by using a piezomotor.

The AFM used during this project is a NTEGRA, the scanning software is Nova, and the scans are treated and analysed using the software WSxM 5.0, which is a tool for scanning probe microscopy [22]. Initially the sample is mounted on the sample holder, which is placed on the stage. Then the scanning software is opened and the laser is guided to hit the cantilever in order to obtain a proper signal. Next the resonance frequency is determined and its magnitude is adjusted. Then, the sample is brought into contact with the scanning tip using the approach feature.

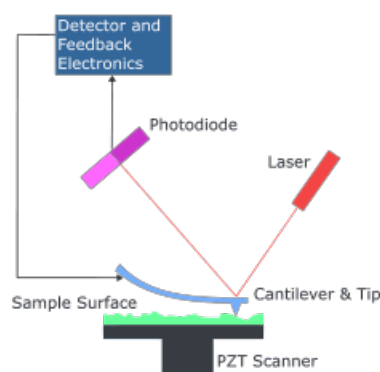


**Figure 3.2:** Schematic of the process in AFM measurements. [21]

Finally, the scan area, the number of points per line, and the scan frequency are set. The number of points per line is in this project set to 512, the scan frequency is set between 0.3 and 0.5 (corresponding to 2-3 seconds per line), and the scan area is varied within the range between  $10 \times 10$  and  $40 \times 40 \mu\text{m}$ . In order to ensure a proper scan quality the surface topography is scanned in both directions, so if the tip is not completely following the surface or if the approach is insufficient, it can be detected.

### 3.4 Fourier transform infrared spectroscopy

Fourier Transform Infrared Spectroscopy (FTIR) is used in order to determine if a chemical substance corresponding to PEG is deposited on the surface of the sapphire substrates, which was used to simulate the filter surface.

A PEG layer with a thickness above 50 nanometers<sup>1</sup> were grown by re-initiating the hydroxy-groups at the end of the PEG with sodium methoxide, and then measure with ellipsometer after each polymerisation.

When the layer was thick enough, the measurements were performed. First, a background spectrum was made. Then the sample was mounted in the holder for transmission spectroscopy, and the holder was placed in the FTIR setup. The sample was then transilluminated, and the spectra were recorded. The number of recordings and the interval between the periods measured could be adjusted in order to optimise the collected spectrum.

<sup>1</sup>This thickness was expected to be sufficient to get a signal with the available equipment

### 3.5 Drop analysis

Drop analysis is used to determine the change in hydrophilicity of the surface. As described in section 2.2, the equation

$$\theta_0 = \cos^{-1} \left( \frac{\Gamma_A \cos(\theta_A) + \Gamma_R \cos(\theta_R)}{\Gamma_A + \Gamma_R} \right),$$

where

$$\Gamma_X = \left( \frac{\sin^3(\theta_X)}{2 - 3 \cos(\theta_X) + \cos^3(\theta_X)} \right)^{\frac{1}{3}}, \quad X = A, R.$$

is used to determine the equilibrium contact angle between a surface and a droplet or bubble.

Throughout this project two methods of contact angle measurement have been used, which are the sessile-drop technique and the captive-bubble method. The sessile-drop technique is the simpler one and is used on the sapphire substrate, but it can not be applied to porous, hydrophilic surfaces, because the water permeates the filter, so a stable water droplet can not be sustained. Thus the filters are characterised with the captive bubble method. The objective with both techniques is to determine the advancing and receding angles.

A simple setup is used to the sessile-drop technique in this project. The sample is placed in the view of the camera, which is connected to a computer with a camera software, IC Capture, that is able to record the camera images with a given time interval. Above the sample is a piece of microtube connected to a syringe containing demineralised water. The syringe is mounted in a syringe pump from where the water feed rate can be controlled. The rate used in this project is  $6 \frac{\mu L}{min}$ .

The software is set to record with one second time interval and the syringe pump is started. A water drop starts forming on the surface and in this initial drop forming the advancing angle is determined. Theoretically the advancing angle should be measurable throughout the drop volume increasing step, however as the volume increases the influence of gravity on the drop becomes more visible as the contact angle decreases with increasing drop volume [23]. As the drop reaches a certain size the feed is stopped and the drop slowly evaporates. According to the theory in section 2.2 the drop will not start receding immediately, because of the line energy, and a contact angle decrease will be observed as the drop evaporates. Finally at some point the drop will start receding and maintain a constant contact angle for a period of time. At this point the receding angle is determined.

For the captive-bubble method, done in this project, the setup described above is modified. A transparent polymethyl methacrylate container is filled with demineralised water and the sample is lowered into it and the bubbles are removed from the bottom surface of the filter. The container is placed directly in front of the camera and the filter is placed in focus. One end of the microtube is fixed

below the filter and the other end of the microtube is connected to a syringe with air. The syringe pump is used to eject a bubble of air with an injection speed of  $6 \frac{\mu\text{L}}{\text{min}}$ . After this, the process is inverted and the bubble must be emptied with the same volume rate. Thereby the advancing and receding angles can be determined. Here it should be noted that as the bubble volume increases the receding angle is measured and vice versa, because the contact angle is defined as the angle between the surface/liquid and liquid/air interfaces.

The image sequences from both methods is then analysed using the imageJ plugin DropSnake, which delivers the contact angles to a given time. From these data the advancing and receding angles can be determined and used in equation 3.2 to calculate Young's equilibrium contact angle.

## 3.6 Flow tests

At the Grundfos test facilities in Bjerringbro, two different kinds of flow tests were performed in order to investigate the anti-fouling properties of the treated filters. A dead end flow test, where two different proteins were dissolved in buffer solutions, was used to see how easy it was to rinse off the proteins. Afterwards a cross-flow test with possibility of back-flush was carried out to see how the filters responded to artificial lake water.<sup>2</sup>

### 3.6.1 Dead end flow tests

The dead end flow tests were performed by leading a solution of protein into an AMICON 8050 cell with a TMP of 0.6 Bar. The solution has to pass through the filter, to end up in a container placed on a weight. The weight was logged with respect to time, so a permeate versus time curve was obtained. A schematic of the setup is shown in figure 3.3.

The buffer was 0.010M sodium phosphate, and the proteins used were bovine serum albumin (BSA) and lysozyme, and it has to be noted that BSA has a lower isoelectric point than lysozyme, and thereby would be uncharged in the solution while lysozyme would be charged.<sup>3</sup>

A sample was mounted in the cell, and extra air was let out. Pressure was applied in order to see if it was tight. Then the collection of data from the weight was started.

---

<sup>2</sup>100 liter artificial lake water contains the following: 3.969 g sodium sulphate, 5.769 g sodium hydrogen carbonate, 12.419 g sodium chloride, 0.011 g kaolite, 5.00 g N<sub>8</sub>-alginat, 6.25 g BSA, and 1.08 g humic acid.

<sup>3</sup>The isoelectric point of BSA is 4.7 [24] and that of lysozyme is 10.9 [25].

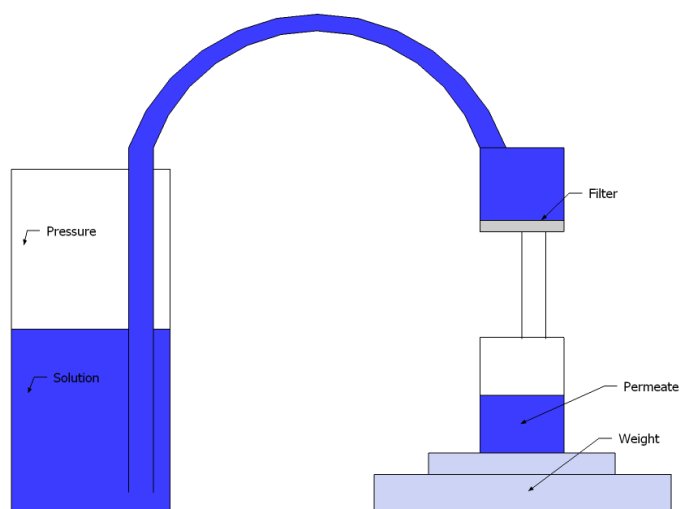


**Figure 3.3:** Schematic of the setup for the dead-end flow test.

First a reference test of the flux of reverse osmosis treated water (RO-water) through the filter was done in order to determine the water flux through the clean filters. Then the filter was tested with one of the protein solutions, to generate the fouling curve. Afterwards they were externally cleaned, by rinsing with more RO-water as well as stored in it until a second RO-water flux test was performed to see the degree of reversible fouling.

After this test, some of the filters were stained in order to see the difference of the adsorption of proteins on the modified as compared to reference filters.

### 3.6.2 Cross-flow tests

A setup to test the anti-fouling abilities is located at Grundfos. TMP, cross-flow speed, temperature, back-flush pressure and back-flush interval can be determined, and set as experimental parameters. A sample was mounted in the setup with both inlet and outlet for cross-flow, flow through the membrane and pressure valves. The experimental parameters were set, and air was let out of the system to prevent noise on the measurements. The process is illustrated in figure 3.4.

First clean water tests with RO-water were performed on all the filters, and they were stored in RO water until the next test. These clean water fluxes are used to compare with the back-flush flux recovery during the experiments.

After this the filters were mounted in order to perform a test with artificial lake water. Two series were made, one with different cross-flow speeds, and one similar, but with back-flush after a time interval as well. After the tests, the filters were stored in RO-water again, and photographed. The purpose with the back-

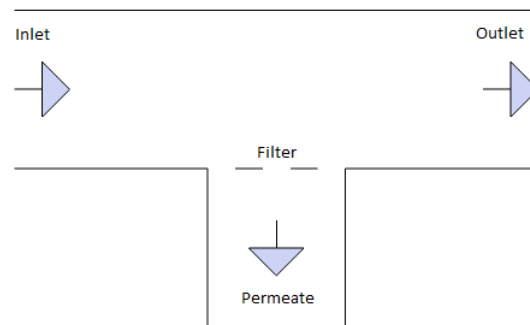


**Figure 3.4:** Schematic of the membrane cell in the cross flow setup. The solution flows parallel to the filter and permeate runs through the filter due to the TMP.

flush sequences is to investigate the fouling reversibility of the treated filters and reference filters by measuring how much of the initial flux that can be recovered.



## Chapter 4

# Experiments and results

*In this chapter the experimental work will be presented. Parallels to the theory and the used methods in previous chapters will be made in order to discuss the results in the correct context. These discussions will be summarised later and used for the conclusion.*

### 4.1 Polymerisation on silicon substrates

To ensure reproducibility of the results of the polymerisations, series of polymerisations on silicon oxide substrates were made according to the procedure described in section 3.1. All polymerisation parameters except the temperature were kept constant during production. The temperature was varied in order to investigate its effect on growth rate and film topography.

The goal of this series was to produce and reproduce smooth, homogeneous PEG films, but also to determine some surface properties of the PEG layer. Characterisations were performed with ellipsometry and AFM.

#### 4.1.1 Ellipsometry

Ellipsometry was used in order to determine the thickness of the polymer layer on top of the thermally grown oxide layer. First the oxide layer was measured alone on the silicon substrate. After polymerisation it was used to determine the thickness of the PEG layer.

In table 4.1 an overview of the samples and the distribution of thicknesses can be seen. Polymerisations were carried out at 110, 125, and 140°C for an hour and the activations at 75°C, also for an hour. Note that these temperatures are measured

Number of samples	Pol. temperature	Avg. layer thickness	Std. deviation
9	110 °C	4.12 nm	0.57 nm
2	125 °C	4.54 nm	0.26 nm
3	140 °C	6.77 nm	1.83 nm

**Table 4.1:** Representative, selected PEG layer thicknesses with polymerisation temperature. All samples in this table have been polymerised for one hour.

in the heat cap on the starfish setup (section 3.1 on page 25), so it might not be the actual polymerisation temperature.

A layer was grown in every polymerisation, though with varying results with respect to thickness.

#### 4.1.2 AFM

AFM measurements were carried out in order to examine the topography of the polymer layer. The roughness was expected to increase slightly, compared to the smooth silicon wafers.

During the polymerisation, beads, expected to be aggregated glycidol, was physisorbed to the surface. In figures 4.1 and 4.2 the difference between a polymerised surface before and after ultrasonic cleaning can be seen. The number of beads has decreased, as have the roughness as can be seen in the captions of the figures. In the surface topography histograms, seen in figures 4.3 and 4.4, it can also be seen that the surface is smoother after the ultrasonic cleaning. The root-mean-square (RMS) roughness dropped from 12.84 nm to 1.59 nm and the average roughness dropped from 4.92 nm to 1.17 nm. This trend was observed on most of the polymerised samples on silicon oxide substrates.

#### 4.1.3 Results from polymerisation on silicon dioxide

In the polymerisation on silicon dioxide, it was shown that it was possible to obtain homogeneous results of the polymerisation with respect to layer thickness and smoothness of the surface. When these results were obtained, it was possible to start the transfer of the process to aluminium oxide substrates, which was a part of the project aim. Furthermore, it provided the possibility to find suitable experimental parameters, which were attempted copied to the later parts of the experimental work, though the setup was changed.

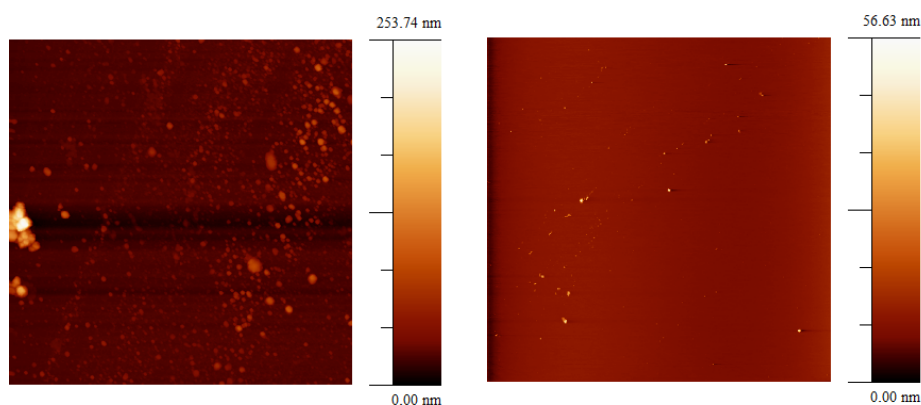


**Figure 4.1:** A representative AFM image of a sample after polymerisation. It is seen that aggregates are formed on the surface, which otherwise is smooth.

**Figure 4.2:** A representative AFM image of a sample after polymerisation and ultrasound cleaning. The surface is smoother than before the ultrasound cleaning.

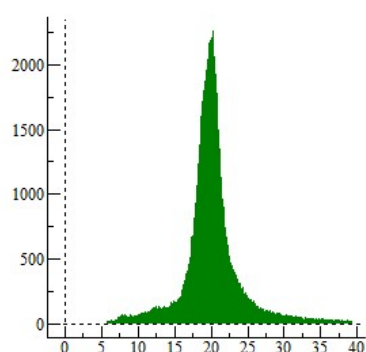


**Figure 4.3:** Surface topography histogram of the sample before ultrasound cleaning. The RMS and average roughness are determined to be 12.8 nm and 4.92 nm using WSxM.

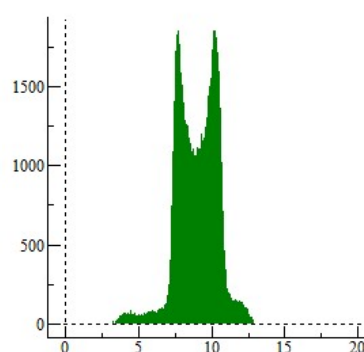


**Figure 4.4:** Surface topography histogram of the sample after ultrasound cleaning. The RMS and average roughness are determined to be 1.59 nm and 1.17 nm using WSxM.

## 4.2 Polymerisation on aluminium oxide substrates

When the process was transferred from silicon oxide to aluminium oxide, experiments were performed in order to show the success of the transfer. Ellipsometry proved a little harder due to the optical properties of the aluminium oxide, hence

statistical studies were not performed. AFM was still performed in order to examine the surface topography, and drop analysis was done to see if one of the aims of the project, to create a more hydrophilic surface, was achieved. IR spectroscopy was also carried out to validate the presence and characterise the PEG film on top of the sapphire substrate.

### 4.2.1 Ellipsometry

In order to use the ellipsometric method on the surface of the transparent aluminium oxide, a sample was polished into a wedge shape. This allowed the back-side signal to radiate in a different angle than the front signal. With this modification made, it was possible to measure the thickness of the PEG layer, though the accuracy tended to be lower, due to the more flat output of the stokes parameters. In addition, the measurements still contained some noise from the polished surface.

The thickness tended to be similar to those obtained for silicon oxide, but due to the change of setup it is not known whether the exact process temperature was the same. It was clearly shown that a layer was grown on the surface. The optical properties matched those of the layer grown on silicon oxide.

### 4.2.2 AFM measurements

In the same way, the properties of the layer proved to be similar with respect to the surface topography. First a clean sapphire substrate was scanned in order to examine its roughness before growing the PEG film. An AFM scan and the surface topography histogram are shown in figures 4.5 and 4.7, where it is seen that it is almost perfectly smooth with an RMS and average roughness of 0.56 nm and 0.40 nm.

Subsequently a PEG film was grown and the sample was again investigated by AFM and the scan and surface topography histogram are shown in figures 4.6 and 4.8. From the image it is clear that something has been deposited onto the surface, and it showed the same pattern as for PEG on silicon oxide substrates. It is likely to be glycidol aggregates that were adsorbed to the surface, as it was removable by ultrasonic cleaning in ethanol. The RMS and average roughness of this sample were 31.97 nm and 23.45 nm, respectively.

### 4.2.3 Infra-red spectroscopy

In order to verify the presence and characterise the polymer layer a PEG layer was grown on a sapphire substrate to be used in FTIR characterisation. Due to the polymerisation process PEG film was grown on both sides of the sapphire sub-

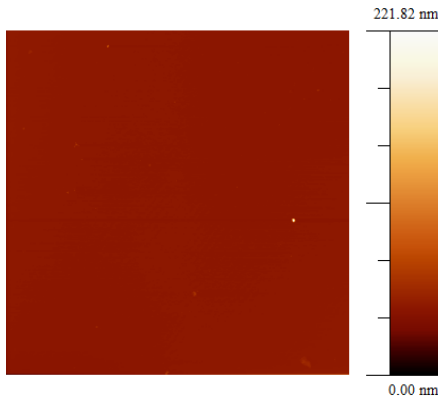


**Figure 4.5:** AFM scanning of a clean sapphire substrate. It seems to be perfectly smooth although a few impurities are present.

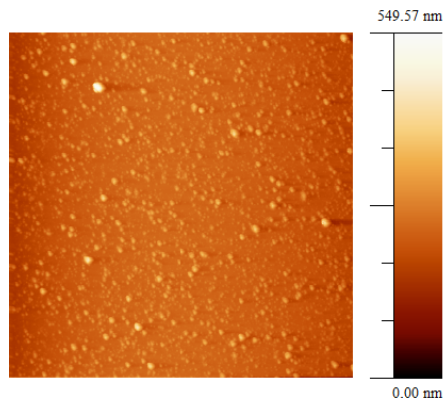


**Figure 4.6:** AFM scanning of PEG on a sapphire substrate. It is seen to contain beady structures as on the silicon oxide substrates.

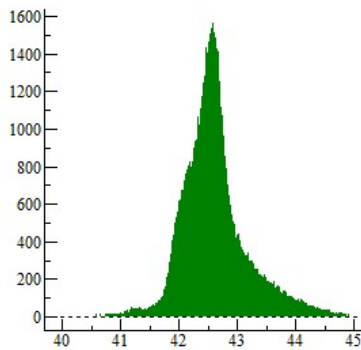


**Figure 4.7:** Surface topography histogram of the clean sapphire substrate. The RMS and average roughness are determined to be 0.56 nm and 0.40 nm using WSxM.

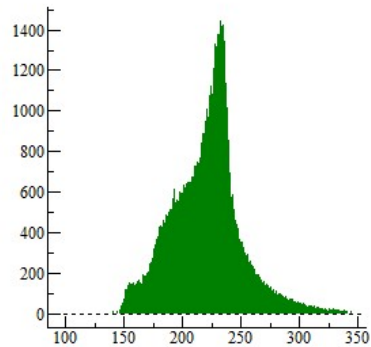


**Figure 4.8:** Surface topography histogram of PEG film on a sapphire substrate. The RMS and average roughness are 31.97 nm and 23.45 nm.

strate. The film thickness was determined by ellipsometry to be 55 nm, which is quite thin, but was expected to be sufficient for infra-red spectroscopy.

Initially, reflection mode was attempted, but discarded because of insufficient signal from the PEG layer and therefore transmission mode was selected instead. At first a reference spectrum was collected, which was a combined result of the

source and vibrational excitations of water vapour and carbon dioxide, because the measurements were carried out in atmospheric air. The reference spectrum is shown in figure 4.9, where it can be seen that the source not only will interact with the sample, but also with water vapour and carbon dioxide in the air. These interactions will not be seen in the characterisation of the samples, because the transmission spectrum is generated by dividing the spectrum through the sample with the reference spectrum in figure 4.9. So assumed that the atmospheric composition stays unchanged in the path of the source, the noise will not be seen in the transmission spectra.

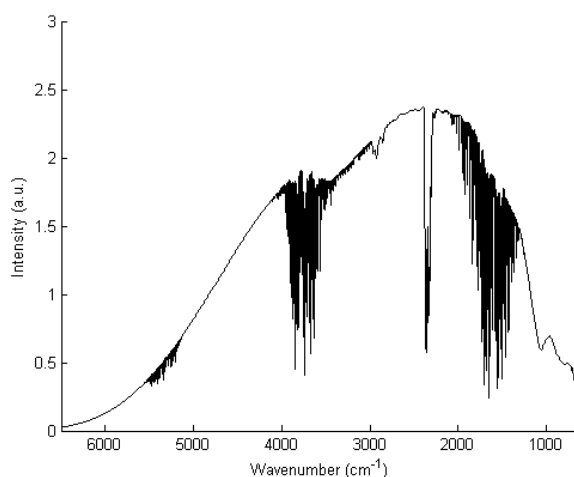


**Figure 4.9:** IR source spectrum through atmospheric air averaged over 120 scans. The noise around  $1700\text{ cm}^{-1}$  and  $3800\text{ cm}^{-1}$  is due to excitation of vibrations in water vapour in the air and the drop around  $2350\text{ cm}^{-1}$  is due to carbon dioxide in the air [18].

After the reference spectrum was obtained, the transmission spectra through the clean sapphire substrate and PEG/sapphire substrate were measured. First the clean sapphire substrate was examined and its transmission spectrum is shown in figure 4.10. It is seen that sapphire has a transmission cut-off around  $1700\text{ cm}^{-1}$ , corresponding to a wavelength of  $5.89\text{ }\mu\text{m}$ , which means that vibrational excitations at wavenumbers lower than this cut-off value can not be detected this way. As mentioned in section 2.4 the wavenumber corresponding to C-O-C stretching lies below  $1700\text{ cm}^{-1}$  and can therefore not be detected. However, the C-H and O-H excitations should still be detectable, since the wavenumbers corresponding to these vibrational excitations are above the cut-off value.

Then the IR transmission spectrum was measured on the sapphire substrate with the PEG film and is shown in figure 4.11. The spectrum follows the same pattern as that of the clean sapphire substrate, but differs around  $2900\text{ cm}^{-1}$  and  $3250\text{ cm}^{-1}$ , where a small drop in transmission is seen. The broad transmission

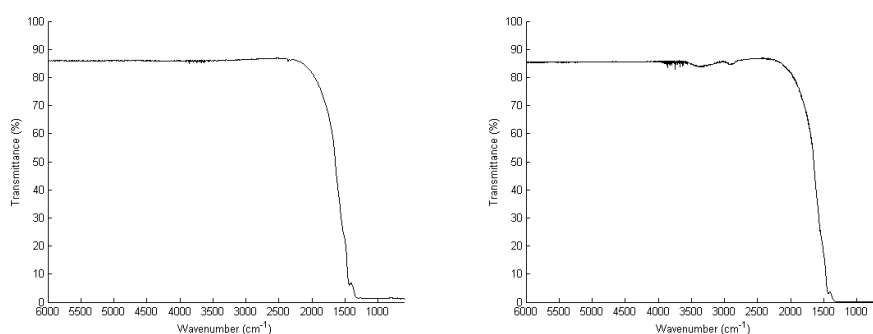


**Figure 4.10:** Transmittance IR spectrum of a clean sapphire substrate. **Figure 4.11:** Transmittance IR spectrum of a sapphire substrate with PEG.

drop around  $3250\text{ cm}^{-1}$  corresponds to vibrational excitation of O-H bonds and the narrow drop around  $2900\text{ cm}^{-1}$  corresponds to vibrations in C-H bonds. A close-up comparison of the two transmission spectra is shown in figure 4.12.

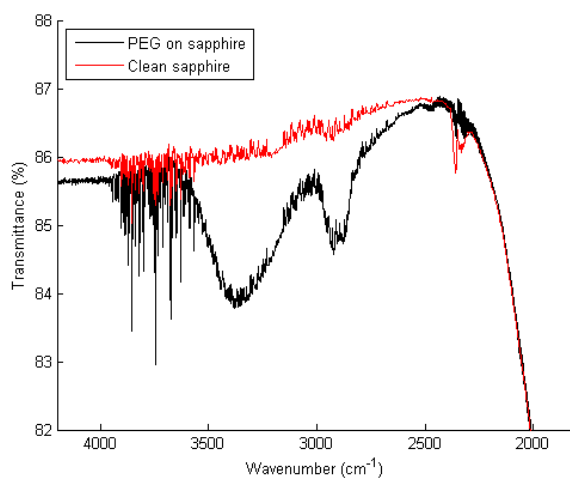


**Figure 4.12:** Close-up comparison of the two IR transmission spectra.

These measurements show that the treatment of a sapphire substrate according to the polymerisation procedure has resulted in a film containing a high concentration of O-H bonds as well as C-H bonds, which suggests that it is an alcohol containing organic film. It is most likely branched PEG, when considering the fact that the monomer used is glycidol and that the only other organic compounds present in the polymerisation procedure are ethanol and methanol. It is also seen that no epoxide is present, meaning that there is no glycidol present in the PEG film.

#### 4.2.4 Contact angle measurements

In order to evaluate the change in surface hydrophilicity contact angle measurements were performed on treated and untreated sapphire substrates and treated and untreated membrane filters. The sapphire substrates were chosen, because it is the same material as the ceramic filters, and should therefore be a good representative to the effect of the surface treatment. On the sapphire substrates the sessile drop technique was used. The procedure for this technique, as well as that of the captive-bubble method, is described in section 3.5.

In both cases the drop/bubble is imaged with a certain frequency, and the contact angles on both sides are measured using the ImageJ plug-in "DropSnake". The contact angle can be plotted as a function of time and the advancing and receding angles can be extracted from the plot. The advancing angle is the angle in the beginning as the droplet volume increases, because the contact angle decreases as the drop volume increases because of the weight of the water. As the droplet slowly evaporates the contact angle decreases, because the edges of the drop is pinned by the triple line energy. However, at some point the drop will begin to recede and the contact angle will remain constant for some time. It is in this time span that the receding angle is measured.

First a control experiment was carried out of a clean sapphire substrate. An image series of the process is shown in figure 4.13 and the contact angle development over time is shown in figure 4.14.

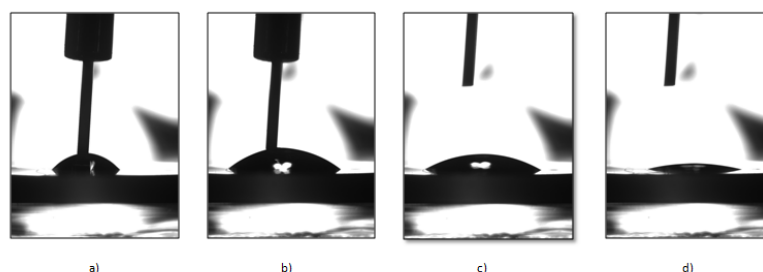


**Figure 4.13:** Images of the water drop. a) The water drop in the beginning of the process. b) Increased volume of the water drop causing a decrease in the contact angle. c) The supply of water is stopped and the droplet evaporates. Notice that the width of the drop has not yet changed due to the line energy. d) The droplet is receding as it evaporates.

From the graph in figure 4.14 the advancing and receding angles can be determined. The advancing angle is read and the receding angle is determined by averaging the contact angle in the receding part of the plot. By inserting these values in equations 2.21 and 2.22 the equilibrium contact angle for water on sapphire is calculated.

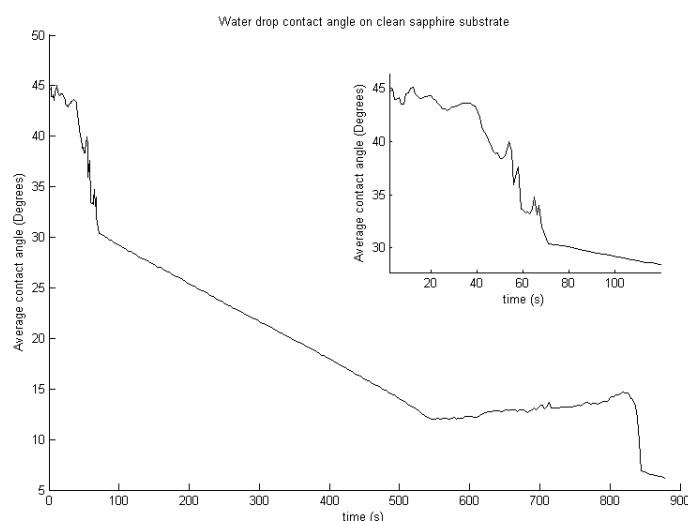


**Figure 4.14:** Water contact angle on clean sapphire substrate. The supply of water stops after 70 seconds and from there the drop slowly evaporates.

Next the same procedure was carried out on a sapphire substrate with a thin PEG-film grown on top of it. Since the goal was to increase the surface hydrophilicity by growing PEG on it, the equilibrium contact angle should decrease if this goal was to be achieved. An image series of this process is shown in figure 4.15, where it can be seen that the PEG layer has made the surface more hydrophilic. The water droplet quickly spread out on the surface and as can be seen in image 4.15a the presence of the microtube seem to disturb the shape of the droplet as opposed to that on clean sapphire.

As can be seen in the image series in figure 4.15, the size of the droplet exceeds the image frame. This makes it unsuitable for contact angle measurements using DropSnake, because this requires that both corners are visible. However, up to the point, where the one triple point exceeds the image frame, DropSnake was used on the images and the average advancing contact angle was determined. The receding angle was a bit more difficult to obtain, because the droplet barely receded before it was fully evaporated. For this purpose another plug-in, LB-ADSA (Low Bond Axisymmetric Drop Shape Analysis), was used. This plug-in fits the Young-Laplace equation to the image of the drop in order to determine the contact angle. It can, however, also be used to determine the contact angle manually, which was done in this case because one drop edge was outside the image frame.

The results of these two experiments are shown in table 4.2, where the effect of the nanometer thin PEG layer clearly shows. The clean sapphire substrate itself was quite hydrophilic with a contact angle of  $29^\circ$ , but the PEG layer made it even more hydrophilic as the equilibrium contact angle was reduced to  $9.6^\circ$ . So the

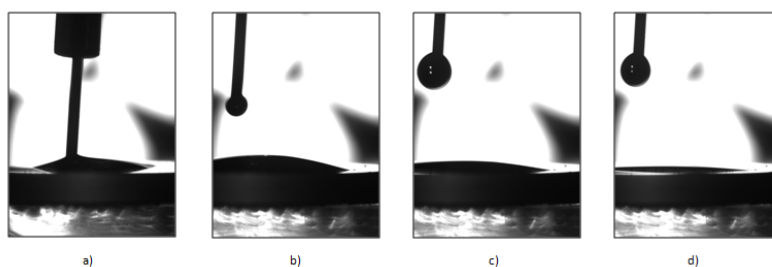


**Figure 4.15:** Images of the water drop on PEG on sapphire. a) The water drop is in the beginning of the process. b) The water drop just after the supply of water stopped and the droplet starts to evaporate. c) The drop is evaporating, but the contact area to the substrate remains the same as the previous image. d) The water drop is at this point beginning to recede.

criterion of making the surface more hydrophilic is fulfilled.

	Adv. angle	Rec. angle	Young's contact angle
Clean sapphire substrate	43.9°	13.0°	<u>29.0°</u>
PEG on sapphire	13.5°	5.2°	<u>9.6°</u>

**Table 4.2:** Advancing, receding, and equilibrium contact angles for clean sapphire and PEG on sapphire.

### 4.3 Polymerisation on filters

After the examination of the results on the sapphire substrates, polymerisations was performed on these membranes, and drop analysis was carried out in order to examine the change in hydrophilicity. The polymerisation procedure was similar to the one described in section 3.1 with one addition. The filter was cleaned ultrasonically in ethanol between the activation and polymerisation step. This was done to remove sodium methoxide from the pores to minimise the risk of polymerisation in the monomer phase in the pores.

#### 4.3.1 Drop analysis

As on the sapphire samples, the purpose of this experiment was to determine the receding and advancing angles in order to determine the equilibrium contact angle of treated and reference filters. This was attempted using the captive-bubble method as described in section 3.5. With the setup used in this project it was not

possible to obtain both the receding and advancing angles because of a delay in the response from the syringe to the end of the microtube, which was not observed in the sessile-drop technique. This is due to water being incompressible, so when the syringe compresses with a given rate water is ejected at the end of the microtube almost immediately with the same rate. On the other hand air is compressible, so when a syringe full of air is compressed with a given rate the pressure builds up inside the syringe. When the pressure is sufficient for the air to overcome the resistance of the microtube air will be let out in the other end of the microtube with an uncontrollable rate. Another obstacle in this process was that in order to decrease the volume of the bubble the end of the microtube should remain inside the bubble, which also was not possible. Finally it was not energetically favourable for the bubbles to stick to the filter surface, meaning that the bubbles were very mobile and could not be kept stationary as their volume increased.

It was managed to capture images of the bubbles, while their volume was increasing and thereby the receding angles on a treated and a reference filter was obtained. The images are shown in figures 4.16 and 4.17, where it is seen that the contact angles look quite similar.

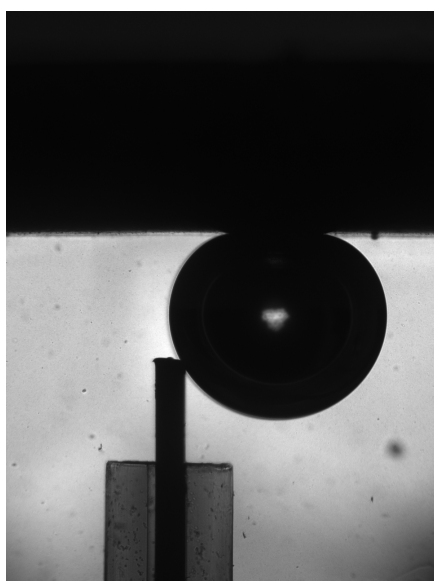


**Figure 4.16:** Air bubble on the bottom of a treated filter submerged in water. The contact angle is the receding angle as the volume is increasing at this point.



**Figure 4.17:** Air bubble on the bottom of a reference filter submerged in water. The contact angle is the receding angle as the volume is increasing at this point.

These images were flipped vertically using ImageJ and the contact angles were measured using DropSnake. The receding angle on the treated filter was measured to be  $8.83^\circ$  and that of the reference filter was measured to be  $16.22^\circ$ . So from

these measurements it seems that the surface treatment of the filters was successful and a PEG film has been grown. However, it does not fully confirm the presence of the PEG film, because of the fact that the contact angle depends on the bubble volume, which may have influenced these measurements.

## 4.4 Hydrodynamic measurements

After successful treatment of the membranes, flow tests were performed in order to examine the effect of the treatment with respect to fouling. The filters were tested in two different setups in order to cover both dead-end filtration and cross-flow filtration. Furthermore the filters were tested with different solutions and different filtration parameters such as the TMP and cross-flow velocity in order to capture the effect of the PEG film on the fouling process.

### 4.4.1 Dead end flowtests

Two series of experiments were performed using the dead end filtration setup, where a BSA solution and a lysozyme solution were used. The same buffer was used to both protein solutions and the solutions therefore had the same pH being around 5. This means that BSA, which has an isoelectric point around 5, was neutrally charged in this buffer and there would therefore be no considerable electrostatic interaction with the membrane surface. However, lysozyme would be charged, because of its isoelectric point being 11. Thereby in the lysozyme series there would also be a more considerable electrostatic interaction between the protein and the surface.

#### BSA filtration

Three treated and two reference filters were tested in this experimental series. Here the purpose was to examine the flux decline during protein filtration and how much of the clean filter water flux that could be recovered by rinsing the filter externally with RO-water. Furthermore the measurements could give an indication to if the treatment had narrowed the pores and thereby decreased the permeability of the filters.

As mentioned in section 3.6 the proteins BSA and lysozyme were used in a sodium phosphate buffer. Initially the clean filter water flux was measured by applying a TMP of 600 mBar and weighing the permeate over time giving a  $V(t)$  dataset. The flux was then obtained by taking the slope of the  $V(t)$  graph. When dealing with fouling curves it is practical to plot the flux as a function of permeate volume, because it gives a clearer picture of the fouling properties. This was there-

fore also used to image the clean filter water flux, which in theory should yield a straight horizontal line. The results of the clean filter water flux tests are shown in figure 4.18, where a small flux decrease can be seen for both treated and reference filters. This might suggest that there have been some impurities in the RO-water and the water flux is therefore taken to be the initial flux of these tests.

Figure 4.18 shows that the flux through two of the three treated filters have decreased about 20%, which indicates that a pore narrowing has taken place. However, the last of the treated samples shows the same flux as the reference filters, which could be caused by an abnormality of the membrane or the fact that the surface treatment of this particular filter had been unsuccessful.

Next, these five filters were tested in BSA filtration, where the BSA concentration was 1g per liter buffer. BSA has an isoelectric point around 5, the same as the buffer pH, meaning that the protein acts as charge neutral in the solution. The results from these tests are shown in figure 4.19.

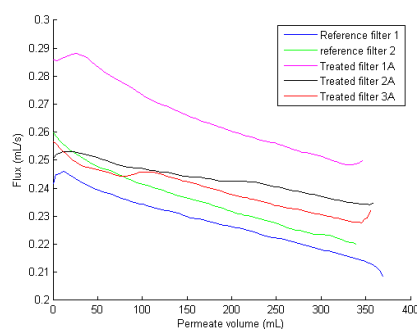
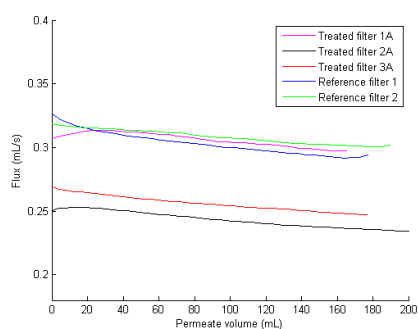


**Figure 4.18:** Water flux through treated and reference filters. **Figure 4.19:** BSA fouling curves for treated and reference filters.

As can be seen in figure 4.19 the rate of flux decrease is quite similar for the treated and untreated filters. This means that the presence of the PEG layer does not seem to have any particular effect on the fouling process for BSA. At least not within the time span of these experiments.

After the BSA filtration experiments the filters were rinsed externally with RO water and kept in RO water to the next day, where the water flux was measured again. Thereby it was possible to determine how much of the original flux that the filters had recovered after being rinsed with water. The results are shown in figure 4.20 and listed in table 4.3.

As can be seen in table 4.3 there is a significant difference in how much of the original flux that was recovered by rinsing the filters with RO water after BSA filtration. The reference filters recovered about 75% of the original flux, where the filters with the PEG layer from 85% up to 98% of the original flux. Furthermore the results indicate that the treatment of filter 1A was successful and that the flux

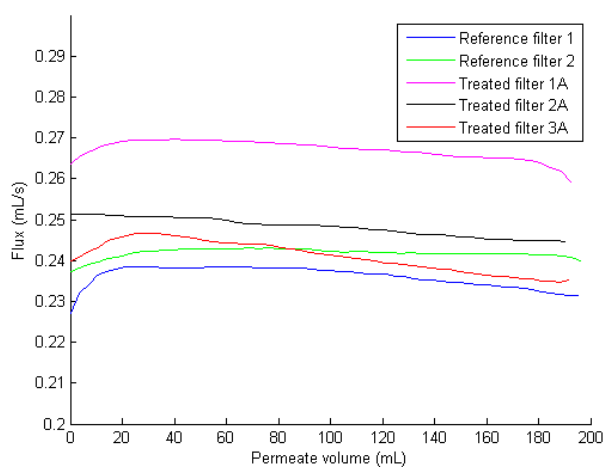


**Figure 4.20:** Water flux measurements on filters after BSA filtration.

Sample	Flux before ( $\frac{mL}{s}$ )	Flux after ( $\frac{mL}{s}$ )	Flux recovery (%)
PEG 1A	0.315	0.270	85.7
PEG 2A	0.270	0.250	92.6
PEG 3A	0.250	0.245	98.0
Ref 1	0.325	0.235	72.3
Ref 2	0.320	0.240	75.0

**Table 4.3:** Water flux on treated and reference filters before and after BSA filtration.

abnormality was likely to be caused by a deviation compared to the other filters.

From the results of this series of experiments it seems that the PEG film does not have any significant effect on the actual fouling process. If any effect should have been observed it would have been that the flux through the treated filters would have decreased more slowly, meaning that the treatment would have favoured the formation of a cake layer more than the reference filters. This was not the case as it was seen that the flux decay of the treated filters are similar to those of the reference filters. This might be due to an insufficient duration of each measurement, but it might also be due to that the BSA fouling process is not affected by the presence of the PEG layer.

The fact that the filter treatment resulted in such an improvement in flux recovery, as the results imply, is promising for the use of PEG anti-fouling nanofilms grown on membrane filters. This is mostly due to the fact that the use of chemical cleaning can be reduced quite significantly.

Usually in order to describe the fouling reversibility, the flux after filter clean-

ing relative to the initial flux is plotted as a function of permeate volume or time. However, in this case the water flux measured in this series was not constant over time due to contaminants in the water or cell. Therefore, as seen in figures 4.18 and 4.20 the water flux through both clean and used filters drop as more water is lead through the filter. The issue with imaging the relative flux is that the water flux of each filter decays differently and a plot of the relative flux would therefore not make sense.

### Protein staining

After having been used in BSA filtration and externally cleaned with water, one treated filter and one reference filter were investigated for their protein surface concentration. This was done by staining the proteins with a fluorophor that binds to the proteins on the surface and the samples were then examined using a fluorescence microscope. Here a high surface concentration of proteins will yield a higher brightness, where a low concentration will yield a low brightness of the signal. The brightness can then be related to the concentration of protein on the surface. The results from these tests are shown in figures 4.21 and 4.22, where the difference in protein surface concentration is clear.

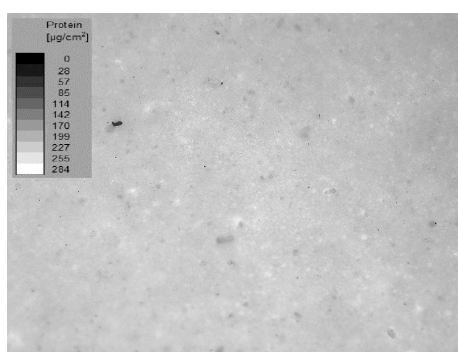
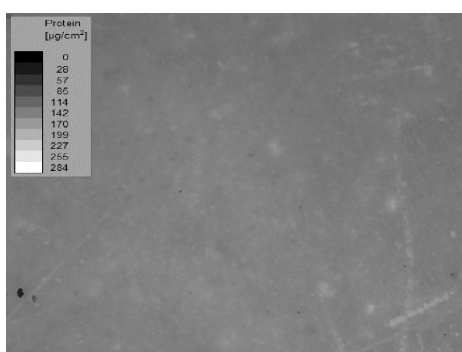


**Figure 4.21:** *Fluorescence microscopy image of stained proteins on treated filter 2A after BSA filtration and external water cleaning.* **Figure 4.22:** *Fluorescence microscopy image of stained proteins on reference filter 2 after BSA filtration and external water cleaning.*

According to the brightness/concentration bars in the images the protein concentration on the treated filter is between 114 and 142  $\frac{\mu\text{g}}{\text{cm}^2}$ , where the concentration on the reference filter is between 227 and 254  $\frac{\mu\text{g}}{\text{cm}^2}$ . In other words, the protein concentration on the treated filter is about half of that on the reference filter. These two filters have been subjected to identical filtration and external cleaning procedures and the only difference between the two filters is the presence of the thin PEG film on the treated filter. This means that BSA is not as compatible to a PEG

coated surface as a clean membrane filter surface, which is an important property in anti-fouling films.

### Lysozyme filtration

A similar experimental series was carried out with a lysozyme solution. Three treated filters and two reference filters were tested in the same manner as the BSA filtration tests. At first the water flux was measured, then the lysozyme filtration was carried out followed by rinsing the filters with RO water, and finally measuring the water flux again.

The water flux tests were carried out and yielded results similar to those in figure 4.18. Again the flux of one of the treated filters was substantially higher than the others, but again this is likely to be caused by the filter properties deviating slightly from those of the other filters.

Next the fouling curves for lysozyme were measured by the same process as for BSA. In this series of experiments it was observed, that the PEG layer has an effect on the fouling process, as can be seen in figure 4.23. The flux plots clearly show that the flux through the treated filters decreases slower than the flux through the reference filters. These results show that the PEG coating had the desired effect, because it has slowed down the flux decrease.

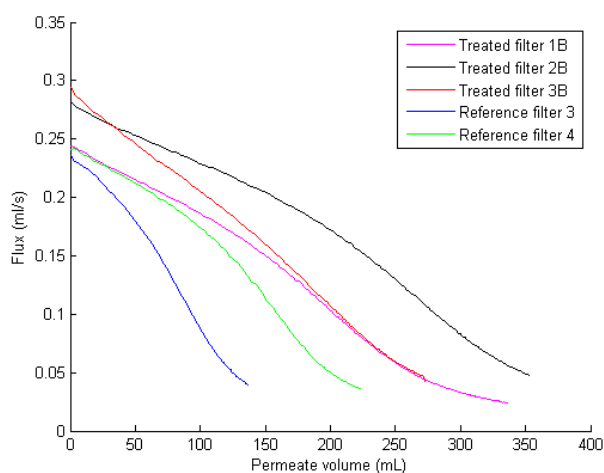


**Figure 4.23:** Lysozyme fouling curves for treated and reference filters.

Another way to clearly see the effect is to plot the permeate volume as a function of time and keep in mind, that it is a small scale experiment. At large scale the filter area is much larger and the TMP will also be higher. Such a plot is for all five samples shown in figure 4.24, where it can be seen that the treated filters have a higher throughput over time than the reference filters, which is an important aspect,

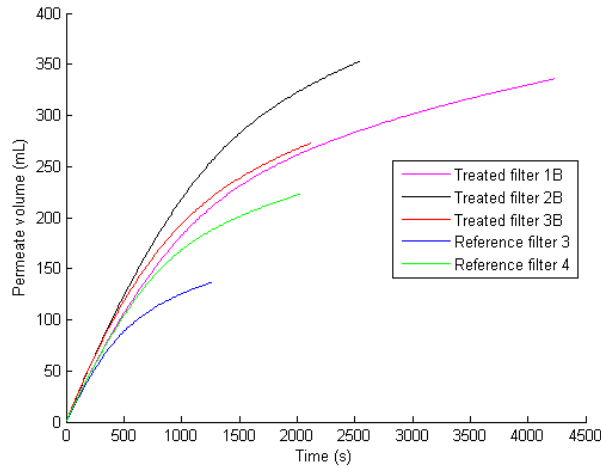


**Figure 4.24:** Throughput over time during lysozyme filtration. Note that sample 1B is run over a longer time period, where it can be seen that the flux seem to have reached a steady state.

when dealing with MBRs. The general characteristic of the throughput profile is that the increase in throughput over time slows down and at some point it reaches a semi-constant flow rate.

Finally the filters were rinsed in RO-water and the water flux was measured again. However, in this series the second water flux tests were carried out the same day, as opposed to the BSA series. Otherwise the filters were given the same treatment as the filters in the BSA series. The water flux results are shown in table 4.4, where it is seen that neither the treated nor the reference filters had recovered much of the original flux. Still it is shown that the treated filters recovered a bit more of the original flux than the reference filters. So if these filters had been cleaned by back flush the effect might have been clearer.

Sample	Flux before ( $\frac{mL}{s}$ )	Flux after ( $\frac{mL}{s}$ )	Flux recovery (%)
PEG 1B	0.278	0.0242	8.71
PEG 2B	0.303	0.0487	16.1
PEG 3B	0.269	0.0458	17.0
Ref 3	0.301	0.0407	13.5
Ref 4	0.280	0.0364	13.0

**Table 4.4:** Water flux on treated and reference filters before and after lysozyme filtration.

All in all based on these two series of flow tests it is seen that the PEG film has

a positive effect as an anti-fouling coating. It increased the ability to remove BSA from the membrane by external water cleaning to a degree that water back-flush might be able to recover the full permeability of the filter, which would minimise the use of chemical cleaning. Furthermore the lysozyme filtration tests showed that the PEG film slowed down the flux decrease in the fouling process, which indicates that cake layer build-up became more dominant over pore blocking and narrowing compared to the reference filters. That being said the fouling process is very complex and depends on a vast number of parameters, both concerning the actual flow and TMP as well as the composition of the solution. Therefore in order to fully validate the effect of PEG as an anti-fouling layer, further testing is needed. However, the results obtained from these tests are promising.

#### 4.4.2 Cross-flow tests

Besides the dead-end flow tests, cross-flow tests were carried out on a larger apparatus, where TMP, cross-flow velocity, and temperatures could be controlled. Initially water flux tests were carried out as dead-end tests, meaning at zero cross-flow and at different TMP over time. The pressure difference was in sequence set to 0.5, 1, 2, 3, and 0.5 bar and the flux was expected to scale linearly with the pressure difference as observed in figures 4.25 and 4.26. Eight samples in total were prepared for this test series; four treated and four reference filters. The water flux test was carried out on all eight samples in order to determine the clean filter water flux and to see if there were any notable difference between the treated filters and the reference filters.

In general it was observed that the treated and reference filters roughly exhibited the same average water flux, which is shown in figure 4.25, where the average water flux for the treated and reference filters are given. It was seen that the treated filters had a slightly higher average flux, but the small difference indicates that it is most likely due to different filter permeabilities.

However, it was also observed that in two of the four treated filters the pores were clogged with a PEG wax. This has been caused by either insufficient removal of sodium methoxide from the pores after activation or to thermal initiation in the pores during polymerisation. It was possible to force the wax out by increasing the TMP during the measurement cycle and afterwards the flux obtained in the second cycle matched those of both the other treated filters and reference filters. The two water flux cycles of this filter are shown in figure 4.26.

Here it is seen that at low TMP (0.5 bar) the flux remains constant and very low, but as the TMP is raised the flux started increasing over time even though the TMP was kept constant in between each TMP shift. This shows that it was a viscous substance, which was not bound to the surface that had blocked the pores. The described situation happened with one more of the treated filters, while the last two treated filters were not blocked.

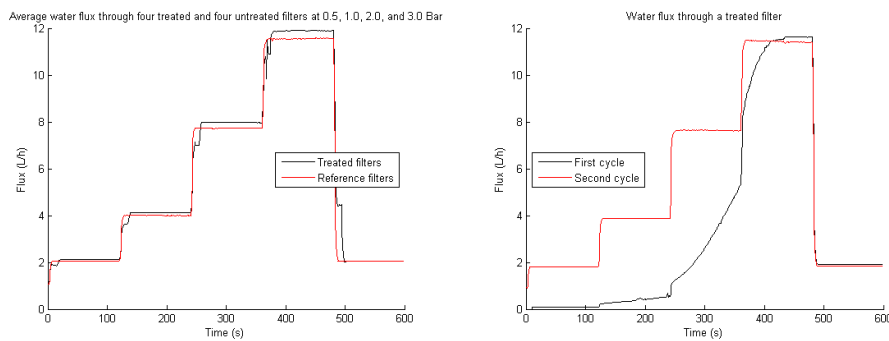


**Figure 4.25:** Average water fluxes for treated and reference filters. **Figure 4.26:** First and second cycle of water flux test of one treated filter.

With the water fluxes obtained the next step was to test the fouling properties of the treated and untreated filters. In these measurements the TMP was kept constant at 1 bar and the cross-flow velocity was altered at a given time interval, starting at  $1 \frac{m^3}{h}$  going to 2, 3, and finally  $1 \frac{m^3}{h}$  again. The flux and cross-flow velocity is plotted as a function of permeate volume in figure 4.27.

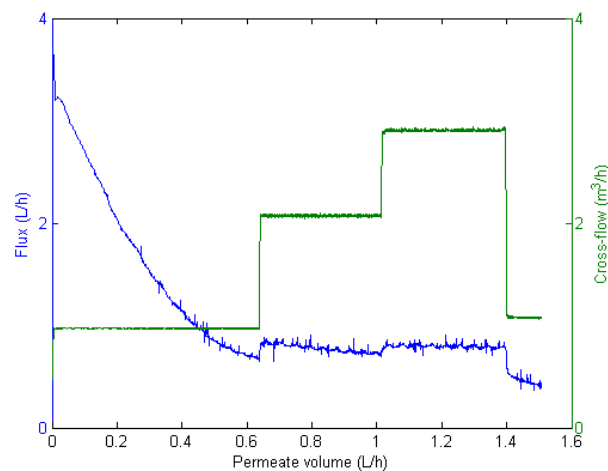


**Figure 4.27:** Flux and cross-flow as a function of permeate volume.

The figure shows that at constant cross-flow the flux drops as expected until the cross-flow is increased. Then, when the cross-flow was increased the flux also increased at the time of the increase and afterwards drops again. The small increase could be due to some of the cake layer being removed by the increased cross-flow velocity.

It can be seen that there is some noise in the measurements, which is caused by air bubbles in the system. This noise is to some extent removable during data treat-

ment, by overwriting the noisy measurements by the average flux of the previous and following measurement. This procedure is done on all the fouling measurements, because they all contained noise to some extent.

Another thing worth noting is the fact that at the higher cross-flows the flux seems to oscillate, meaning that the cake layer thickness is oscillating. Theoretically this should not happen, because at a constant cross-flow velocity the critical cake layer thickness should remain constant as well. However, by zooming in on the cross-flow and flux respectively as the cross-flow is at  $3 \frac{m^3}{h}$  it can be seen that there are some periodical fluctuations in the cross-flow, which increases and decreases the critical cake layer thickness and thereby also the flux over time. These plots are shown in figures 4.28 and 4.29, where it is seen that the cross-flow fluctuations are very small (about 0.3%) and the flux fluctuations are quite large (about 4%) compared to their average values. There might therefore be another reason to these flux fluctuations.

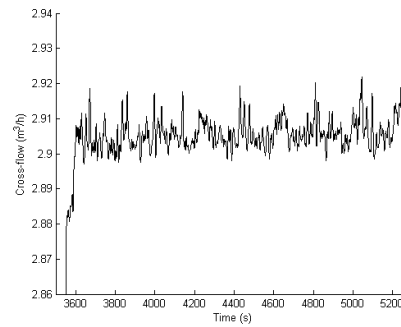
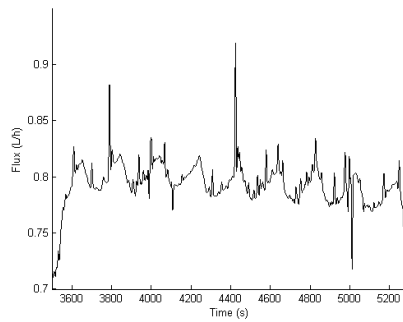


**Figure 4.28:** *Oscillations in flux over time.* **Figure 4.29:** *Oscillations in cross-flow over time.*

In order to investigate the fouling characteristics, but also the fouling reversibility, a test sequence involving back-flush cleaning of the filter was introduced. In back-flush cleaning the feed is closed and clean water flows through the filter from the back side in order to physically remove the filtrate from the simulated lake water on the filter. The total sequence is designed such that the system runs three cycles as described in figure 4.27 with six minutes cross-flow time intervals and still with a constant TMP of 1 bar. In between the three main cycles one minute of back-flush cleaning is introduced in order to detect any difference in fouling reversibility due to the PEG layer. It is measured by how much of the original water flux that is recovered by back-flush cleaning. Because of the dead zone on the filter it is not expected that the flux is fully recoverable, because only 60% of the filtration area is subjected to back-flush cleaning. Therefore the optimal result must be to recover 60% of the clean water flux.

In this experimental series two treated and two reference filters were investigated with the procedure as described above. The results are shown in figures 4.30

and 4.31.

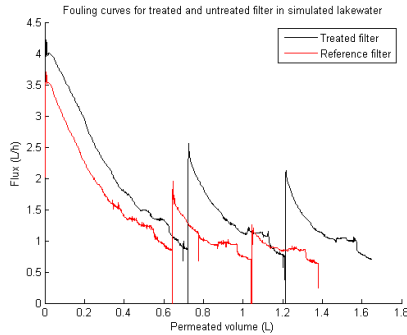


**Figure 4.30:** Flux through the filter as a function of permeate volume for treated filter 3 and reference filter 3.

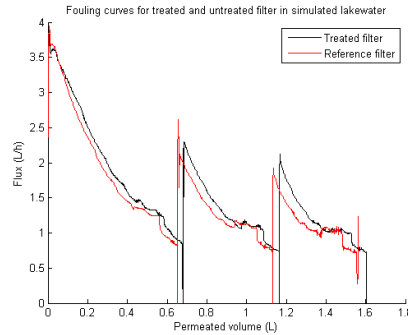


**Figure 4.31:** Flux through the filter as a function of permeate volume for treated filter 4 and reference filter 4.

The results in this series show that the fouling process is quite similar for the treated and untreated filters. However, there is a difference in how much of the original water flux that is recovered after the back-flush cycles. Also it is worth noting that reference filter 3 seem to start at a lower flux even though the clean water flux tests showed that the two filters had the same flux of  $4 \frac{L}{h}$  at a TMP of 1 bar. This could indicate that the foulants can more easily attach to the reference filter surface during a cross-flow filtration test causing a fast drop initially, but there might be other reasons to the difference in initial flux.

The interesting part is the fact that the flux recovery of both treated filters is considerably better than that of reference filter 3 and a little better than that of reference filter 4. The initial and recovered fluxes are read from the two plots and listed in table 4.5, where the clean water fluxes are collected from the initial water flux tests.

Sample	Clean water flux ( $\frac{L}{h}$ )	First recovery ( $\frac{L}{h}$ )	Second recovery ( $\frac{L}{h}$ )
PEG 3	4.23	2.46	2.05
PEG 4	4.22	2.29	2.08
Ref 3	4.18	1.67	1.17
Ref 4	4.04	2.11	1.87

**Table 4.5:** Initial water flux and recovered fluxes due to back-flush cleaning. PEG 3 and PEG 4 refer to the treated filters 3 and 4, and Ref 3 and Ref 4 refer to the reference filters 3 and 4.

As can be seen in table 4.5 the PEG layer on the treated filters yields a higher fouling reversibility on the samples used in this test. However, in order to fully

confirm or disprove the effect of the PEG layer a larger sample size is needed. The results obtained in this series, along with the results from the dead end flow tests, indicates that a nanometer thin PEG film grown directly on the surface of a membrane filter has a positive anti-fouling property. So if the process of treating the filter surfaces could be made more efficient with respect to chemical use and man-power costs, this filter treatment could in the long run decrease the costs of operation and chemical cleaning in a way that financially would be worthwhile.

# Chapter 5

## Discussion

*In this chapter, relevant discussions of the results in this report will be presented. Relevant parallels will be made between the theory and the results, and the places where it differs and agrees will be highlighted.*

### 5.1 Silicon dioxide

The polymerisations on silicon dioxide were performed in order to replicate the procedure used by Khan et al., in order to replicate both the results and the procedure before the transfer of the process to aluminium oxide. This was succeeded, to some extent, though some differences were observed.

#### 5.1.1 Results compared to Khan et al.

Results similar to those of Khan et al. were obtained, even though parameters had to be varied considerably. This might be due to differences in setups and methods. It was intended to obtain a similar growth rate as that obtained by Khan et al. Many of the experiments in Khan's article were not replicated either, though it might be interesting if further work were to be performed. Especially, to ensure homogeneity the experiments about growth rates could be wise to perform if the technology were to be used in industrial productions.

#### 5.1.2 Process parameters

The difference between the results obtained by Khan and this report can be founded in several places, but a possible explanation could be variations in the actual pro-

cess temperature. In this report, the temperature of the starfish setup, explained in section 3.1, used for the initial setup is different from the temperature of the setup with the oil bath, and furthermore one of the processes were performed under pressure, the other with reflux. These parameters could be interesting to evaluate in order to get the optimal setup, but as far as this experimental work has shown, both are able to produce PEG layers. The later setup proved to produce a polymer wax under, so far, unknown circumstances, but this might be a result of the increased volume of glycidol, where vapour could be responsible for the polymerisation in the first setup with the small volume.

### 5.1.3 Cleaning and possible problems

The wax formation was a continuous problem in the experimental work in later parts of the project, independent of substrates, and in the earlier parts of the project it also proved that activation could be a problem. Both of these effects could be contributed to insufficient cleaning of the glassware, since later on in the process cleaning in nitric acid proved to be effective. It could mean that the amorphous surface of the glassware was initiabile as well, and the polymer layer produced here could be reinitiated more favourably than the substrate of aluminium or silicon oxide.

### 5.1.4 Multi-wavelength ellipsometry and models for refractive indices

A major difference between the methods of Khan et al. and the methods presented in this report is the use of ellipsometry. Khan used the technique of single-wavelength ellipsometry, with a refractive index measured on bulk-polymerised PEG. In this report, multi-wavelength ellipsometry was used, and the refractive index was found through a model for linear PEG given in [20].

Where the method with respect to the refractive index is more accurate in the method presented by Khan et al., the method of ellipsometry is less powerful than the one used in this project. The fit to the Stokes parameters in single-wavelength ellipsometry is not as efficient, due to the lack of data points, thus the accuracy of the fit of the thickness will decrease.

## 5.2 Aluminium oxide

One main goal of the experiments on aluminium oxide substrates was to transfer the process from the silicon oxide surface and onto a surface similar to the one of a commercially available filter. The transfer of the process took place without any major difficulties, though some of the measurements proved to be problematic. The

growth-rates on the new substrate might differ from these on silicon oxide, though it was hard to conclude due to the small sample size.

### 5.2.1 Ellipsometry

Ellipsometry proved to be difficult on the transparent sapphire substrate. The backside signal from a transparent, smooth surfaced substrate is as strong as the front side signal, and with a thickness in the range of a millimeter, and the polymer layer a few nanometers, the fit becomes impossible.

This problem was solved by polishing the substrate into a wedge-shape. By changing the angle, the backside signal could be reflected to another spot than the front site signal, but due to the lower quality of the polished surface, and the hardness of the aluminium oxide, noise still interfered with the signal, though not more than a set of stokes parameters could be obtained and used.

When a fit to the Stokes parameters of PEG on aluminium oxide were made, it could also be seen that ellipsometry not is as powerful a tool in this composition as on silicon oxide. The Stokes parameters tended to be smooth curves, making the fitting hard to do, since no peaks were located in the measured spectrum.

### 5.2.2 Infrared spectroscopy

The results of the infrared spectroscopy clearly indicate that something organic is present on the surface of the aluminium oxide window, though it is not clear what it is. The cut-off from the substrate makes it impossible to detect the presence of ether-bonds, and with that thin a layer, reflective measurements were not possible.

With the added substances and results of Khan et al. in mind, it is hard to suspect other things than branched PEG to be present, though. A direct conclusion might need other methods or a thicker PEG layer.

## 5.3 Drop analysis

The drop analysis experiments were performed in order to confirm an increase in the hydrophilicity of the surfaces, when they were coated with PEG. It was attempted both on the filters and the aluminium oxide substrates.

### 5.3.1 Aluminium oxide substrate

The aluminium oxide substrates, with their reflective, solid, surface were tested with both drop and captive bubble analysis. For very hydrophilic surfaces, captive

bubble analysis would be advisable, though a more complicated setup is needed.

### **Sessile-drop analysis**

The drop analysis technique is easy to adapt, and the flow rate of the syringe pump is easy to adjust. Therefore, this was the technique used in the initial experiments of the hydrophilicity of the surface. It also proved to be the best technique, even though some flaws could be found.

With the exceptionally hydrophilic surface produced in this project, the disturbance from the needle will cause the drop to change shape. This was tried to be avoided by the choice of micro-tubing, but effects must be expected. The same microtube was used in all experiments, so within this report, they should be comparable.

Another challenge was the very small receding angle, which causes some uncertainty in the results. Mostly the software could determine the angles, but as the surface became close to parallel to the substrate, this became harder. Thus the actual angle might differ from the measured, but again this error is expected to be found in all experiments using this setup, meaning that the results should be inter-comparable, but caution should be taken if external comparisons should be made.

### **Captive bubble analysis**

The captive bubble analysis was tried on the aluminium oxide substrate, in order to investigate the properties of the technique. The power of it is no higher for superhydrophilic surfaces, due to the very small contact angle, and it also proved that the build-up of pressure in the microtube, and the sudden release of bubbles was a problem in order to determine a receding angle.

### **5.3.2 Filters**

If a measurement of the change in hydrophilicity on the filters was to be performed, captive bubble analysis had to be used. If the sessile-drop technique was tried on the porous filters, the water would run right through them. It was not possible to expand a bubble with a stable rate though, and due to this, only the receding angle could be analysed since the bubble was expanding. This method is very qualitative, and can only give a difference between the filters, treated and untreated, not the exact changes in surface energy.

## 5.4 Filtration and flow

The topic of the treatment of the filters and the test of the anti-fouling abilities is an extension to the work performed by other groups. No sources were found for work with comparable results, so this work has to be evaluated on its own.

The filtration experiments were performed in order to get an overview of the anti-fouling abilities. They were performed with protein solutions, which might not resemble the usual fouling process entirely, due to the lack of extracellular polymeric substances, but should be a good substitution for the conditioning layer.

### 5.4.1 Polymerisation on filters

The polymerisation on the filters was one of the main goals of the project. The transfer of the process was validated in each step as described earlier in this chapter. No real validation could be made of the presence of the layer on top of the filter, due to the porosity of the surface. Indications could be found through the change of their surface, with drop analysis or direct measurements of the anti-fouling abilities.

The simple method of polymerisation used in this part of the project has both up and downsides. The amount of control of the process is limited to the control of the oil bath, and the only other available parameter is the polymerisation time. The actual process temperature is especially critical, since the temperature of the oil bath might be inhomogeneous. The absence of flow through the cell could also lead to contamination of the polymerisation or activation processes.

All these things combined mean that pore narrowing or blocking can not be eliminated as an error.

### 5.4.2 Dead-end filtration

The dead-end filtration tests were performed on two different proteins with different isoelectric points. This means that the anti-fouling abilities differ for the two proteins, the one charged and the other charge neutral.

The cleaning procedure was different due to time limitations. This entails that the results are not directly comparable, but the difference between the reference filters and the treated filters should be representative.

## BSA

BSA has an isoelectric point at 5, which makes it charge neutral in the buffer solution. Due to this it is expected that there will only be a weak (if any) electrostatic

interaction between BSA and the surface both for treated and reference filters, because both of these surfaces also are uncharged.

**Fouling rate** From the results obtained in this series of experiments, there was not detected any significant difference in the fouling rate to which there could be different reasons. First of all it could be that the presence of the PEG layer simply did not have any effect on the fouling process, which further might be caused by the lack of significant electrostatic interaction between protein and surface. Another explanation could be, that the duration of the experiments was insufficient, as the flux only was allowed to drop to 75% of its original value, where that of lysozyme filtration dropped to only 10%. If the test had been run for a longer period of time there might have been a notable difference in fouling rate.

**Cleaning** The external cleaning was performed by rinsing the samples with RO-water, and then storing them in water for approximately 20 hours. Especially the rinsing might have different effect from sample to sample, since it was performed manually. Pressure and homogeneous cleaning might change from sample to sample, so the results of the cleaning have to be very pronounced in order to be safe to conclude on.

### Lysozyme

The lysozyme has an isoelectric point which makes it charged in the buffer solution. Thereby it is expected that there has been a stronger electrostatic interaction between protein and surface, compared to the BSA filtration experiments.

**Fouling rate** In this series of experiments it was seen that the fouling rate on the treated filters was lower than on the reference filters, as the flux decreased faster on the reference filters. It was also seen that the flux decrease was much faster during lysozyme filtration than during BSA filtration, which is most likely due to the increased electrostatic interaction between protein and surface. The reason for the slower flux decrease on the treated filter might be due to PEG not being as polarisable as aluminium oxide, which results in a lower interaction strength between PEG and lysozyme.

**Cleaning** The external cleaning was performed by rinsing the samples with water, and then storing them in water for 4 hours. The shorter storage in water makes it impossible to make direct parallels between the lysozyme and the BSA cleanings, though the relative degree of flux recovery might be compared if caution is taken. Furthermore only a small percentage of the original flux was recovered from this cleaning method both for the treated filters and reference filters. A more thorough

cleaning method might have yielded a clearer picture of the effect of the PEG layer on the flux recovery.

### **5.4.3 Cross-flow tests**

The cross-flow tests were performed on a setup built to the Grundfos test site, meaning that the results are not directly comparable to results obtained on other setups.

#### **30 minutes cross-flow steps**

The first test series, with the 30 minutes cross-flow plateaus, was performed in order to get an overview of the influence of the cross-flow on the fouling as well as investigating if the PEG film had an effect on the fouling process. If the PEG film had a positive effect on the actual fouling process this would have showed by a lower fouling rate. The experiments provided quite similar results, due to the influence of cross-flow on fouling, where only the cake-layer should be affected. The effect on the cake layer was shown by the flux increase that was seen as the cross-flow velocity was increased.

#### **Back-flush tests**

The second series was performed with back-flush in between shorter steps. These experiments should provide an image of the reversibility of the fouling, due to the back-flush. Furthermore, it should be the closest this project could get to an implementation in a real setup, where simulated lake water and back-flush after a time interval should resemble a MBR setup. A larger sample size should be used if the significance of the change in the anti-fouling abilities should be verified, though.

#### **Dead-zone on the filters**

It was seen on the filters used in cross-flow filtration, that there is an area near the edges of the filters that is darker than the rest of the used filters. At first it was assumed that it was caused by back-flushed area being smaller than the filtration area, but since the pattern also was seen on the filters that had not been back-flushed, this theory was discarded. It is assumed that the cross-flowing lake water simuli is not 'hitting' the entire filter as the lake water enters the filtration chamber at an angle instead of parallel to the filter as was shown in figure 3.4. A photo of the filters used in the cross-flow tests is shown in figure 5.1, where it is seen that the dead zone is present on all the filters.

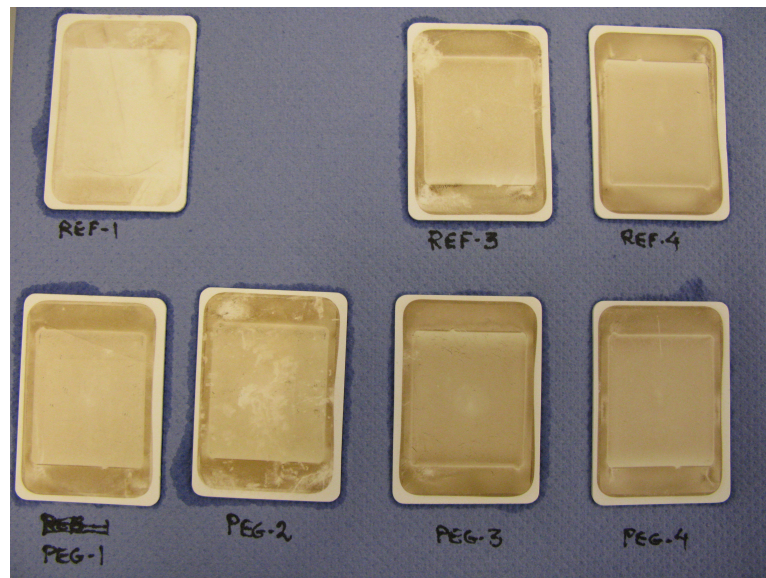


**Figure 5.1:** A photo of the filters used in the cross-flow tests. The filters marked Ref1, PEG1, and PEG2 underwent the procedure described in figure 4.27 and was thereby not back-flushed. The rest of the filters underwent the procedure containing back-flush.

## Chapter 6

### Conclusion

It was managed to grow a nanometer-thin PEG film on a commercially available, ceramic membrane filter with a controlled thickness. Initially it was carried out on silicon oxide surfaces and the method was successfully transferred to solid sapphire substrates and aluminium oxide membrane filters without significant pore narrowing. However, some filters were clogged with a PEG wax from the polymerisation procedure. This could be removed by forcing water through the pores, which resulted in full clean water flux.

The procedure yielded consistent results and the treatment was reproducible. Successful transfer from silicon to aluminium oxide was verified through infra-red spectroscopy and the increased hydrophilicity caused by the presence of the PEG layer was verified through drop analysis.

The PEG film was tested for its anti-fouling properties and the tests yielded promising results. The PEG film caused a higher degree of reversibility for BSA adhering to the filter surface, where close to full permeability was obtained solely by external water cleaning after BSA filtration. The results from the protein staining of the BSA fouled filters also revealed a considerably lower protein concentration on the treated filter after external water cleaning compared to the reference filter.

During lysozyme filtration a slower fouling rate was observed, indicating that cake layer build-up has become more dominant over pore blocking and pore narrowing due to the PEG film. This favourisation of cake layer filtration results in a higher throughput over time, because the flux reduction caused by the cake layer is not as rapid as that of for instance pore blocking.

In the cross-flow tests with simulated lake water, it was seen that the PEG film increased the reversibility of the fouling process, since a higher percentage of the original water flux was recoverable through back-flush cleaning of the filter.

To conclude, the nanometer thin PEG film can be grown directly on the surface of a ceramic membrane filter without any significant decrease in filter permeability. Moreover, due to the results obtained from polymerising on silicon oxide it can be concluded that the procedure is reproducible, which is important in a potential large scale implementation of this procedure. Finally from the fouling tests it can be concluded that the PEG layer exhibited anti-fouling properties, but also that a larger sample size is needed in order to fully confirm these anti-fouling properties.

## Chapter 7

# Perspectives

*In the previous chapters, the experimental work in this report and the relevant theory have been described. This chapter will contain the thoughts of the authors with regard to future perspectives, and the work that would be relevant, if the project should be extended or resumed later.*

In immediate continuation of this project, more experimental and theoretical work could be done.

### 7.1 Future works

First of all, it is recommended that a more thorough characterisation is performed, both with respect to composition and properties of the polymer layer, but also with respect to the anti-fouling abilities.

Detailed studies of the activation process could provide greater knowledge of the attachment between the film and the surface. The degree of activation might also be controllable, which could lead to optimised chemical bonding and controlled polymerisation.

Regarding the polymer layer, many analysis methods could be applied, but to the thin layers transmission electron microscopy would be ideal, being one of the only morphology techniques available for thin layers. X-ray techniques could be applied as well, in order to determine the degree of crystallinity in the polymer phase. By changing the polymerisation conditions, this parameter could be tuned in order to modify the properties of the polymer film.

The anti-fouling properties should be investigated more detailed, in order to obtain a significant, statistical, knowledge of the benefits of the coating of ceramic filters with PEG. Different production parameters could affect the effect significantly, and this should be studied as well.

Further treatment of the polymer layer, with reinitiating, cross-linking and co-polymerising could also be interesting, in order to change the properties of the polymer surface.

By reinitiating the surface, and adding monomers able to react with an  $O^-Na^+$  termination a block-polymer can be composed. This block polymer could change the surface properties from very hydrophilic to hydrophobic, induce less or more binding sites for certain molecules and change the optical properties. This could enable the technique to be used in many other applications than just anti-fouling.

Co-polymerisation is in the same league as re-initiation and block-polymerising, where two monomers similar to glycidol could be mixed in order to form a less homogeneous film. Though it might not be favourable in anti-fouling perspectives, it could be an experimental addition of interest.

Cross-linking could be used to increase the durability of the film, if it proves to be easily worn out. By adding a cross-linking agent, able to react with the alcohol groups and form ethers, a tougher material could be obtained. This could be useful if the environment of the application was tougher than what a normally grown film could handle.

Furthermore, work could be done in order to optimise the process to large scale production, where critical temperatures, maximum humidity and other parameters could be examined. Whenever the chemicals used are reusable by treatment in series could also be interesting, and ways to test this would be beneficial if the process had to be transferred to large scale production.

## 7.2 Potential uses of the process

The polymerisation process of PEG on top of a crystalline ceramic oxide as it is, even without modifications of the process, shows some promising properties which can be applied in various applications. Of course there is the waste-water treatment, described in this report, and other filtration tasks, but other surfaces might as well benefit from the treatment.

One possibility, not far from the anti-fouling of filters, could be to apply a film to piping, in order to prevent the growth of dense biofilms in water systems. A PEG layer combined with the flow through the system could decrease the growth of this biofilm, and by that extend the lifetime of the tubing, or increase the purity of the water passed through.

As very hydrophilic surfaces can be cleaned very easily, in many cases just washing with pure water, the film could be applied to various surfaces, where rain or other frequent watering takes place, in order to keep the surface clean.

The process should be adaptable to most oxides, as long as they are hydroxyl-

terminated and are resistant to strong bases. This means that many ceramic surfaces could benefit from the technique, and combined with, for instance, the techniques described in the last section new material properties can be given to these.



# Bibliography

- [1] Norman N. Li, Anthony G. Fane, W. S. Winston Ho, and T. Matsuura. *Advanced Membrane Technology and Applications*. Number 978-0-471-73167-2. Wiley, first edition, 2008.
- [2] Wenbo Yang, Nazim Cicek, and John Ilg. State-of-the-art of membrane bioreactors: Worldwide research and commercial applications in North America. *Journal of Membrane Science*, 270:201–211, August 2006.
- [3] America's Authority in Membrane Treatment. Membrane bio-reactors. [http://www.amtaorg.com/amta\\_media/pdfs/13\\_MBR.pdf](http://www.amtaorg.com/amta_media/pdfs/13_MBR.pdf).
- [4] Grundfos. Grundfos biobooster. [http://grundfos-biobooster.com/downloads/Biobooster\\_brochure.pdf](http://grundfos-biobooster.com/downloads/Biobooster_brochure.pdf).
- [5] J.I. Gersten and F.W. Smith. *The Physics and Chemistry of Materials*. Number 0-471-05794-0. Wiley New York, 2001.
- [6] In-Soung Chang, Pierre Le Clech, Bruce Jefferson, and Simon Judd. Membrane Fouling in Membrane Bioreactors for Wastewater Treatment. *Journal of Environmental Engineering*, 128-11:1018–1029, November 2002.
- [7] Uma Shankar Singh and Kiran Kapoor. *Microbial Biotechnology*. Number 978-93-801-80179-24-7. Oxford, first edition, 2010.
- [8] Emanuele Ostuni, Robert G. Chapman, Michael N. Liang, Gloria Meluleni, Gerald Pier, Donald E. Ingber, and George M. Whitesides. Self-assembled Monolayers that Resist the Adsorption of Proteins and the Adhesion of Bacterial and Mammalian Cells. *Langmuir*, 17:6336–6343, June 2001.
- [9] John R. Reitz, Frederick J. Milford, and Robert W. Christy. *Foundations of Electromagnetic Theory*. Number 0-201-52624-7. Addison Wesley, 4th edition, 1993.
- [10] Majad Kahn and Wilhelm T. S. Huck. Hyperbranched Polyglycidol on Si/SiO<sub>2</sub> Surfaces via Surface-Initiated Polymerization. *Macromolecules*, 128:5088–5093, May 2006.

- [11] Sadhana Sharma, Robert W. Johnson, and Tejal A. Desai. XPS and AFM Analysis of Antifouling peg Interfaces for Microfabricated Biosensors. *Biosensors and Bioelectronics*, 20:227–239, September 2004.
- [12] W. R. Bowen, J. I. Calvo, and A. Hernández. Steps of Membrane Blocking in Flux Decline during Protein Microfiltration. *Journal of Membrane Science*, 101:153–165, November 1995.
- [13] Donald F. young, Bruce R. Munson, Theodore H. Okiishi, and Wade W. Huebsch. *A brief Introduction to Fluid Mechanics*. Number 978-0-470-03962-5. John Wiley and Sons, fourth edition, 2007.
- [14] Rafael Tadmor. Line Energy and the Relation between Advancing, Receding, and Young Contact Angles. *Langmuir*, 20:7659–7664, March 2004.
- [15] Steven S. Zumdahl and Susan A. Zumdahl. *Chemistry*. Number 978-0-618-52844-8. Houghtin Mifflin, seventh edition, 2007.
- [16] J. Grodzka and A. Pomianowski. Wettability versus Hydrophilicity. *Physicochemical Problems of Mineral Processing*, 40:5–18, 2006.
- [17] Malcolm P. Stevens. *Polymer Chemistry an introduction*. Number 978-0-19-512444-6. Oxford, third edition, 1999.
- [18] M. Hesse, H. Meier, and B. Zeeh. *Spektroskopische Methoden in der Organischen Chemie*. Number 3-13-576102-9. Georg Thieme Verlag, 1984.
- [19] Trinity College Dublin. Ellipsometry.  
<http://www.tcd.ie/Physics/Surfaces/ellipsometry2.php>.
- [20] J. V. Ford, B. G. Sumpter, D. W. Noid, and M. D. Barnes. Refractive index dispersion functions of solid-phase polymers by multicolor optical diffraction. *Applied Physics Letters*, 4:2515–2517, August 2009.
- [21] Wikipedia. Atomic force microscope block diagram.  
[http://upload.wikimedia.org/wikipedia/commons/7/7c/Atomic\\_force\\_microscope\\_block\\_diagram.svg](http://upload.wikimedia.org/wikipedia/commons/7/7c/Atomic_force_microscope_block_diagram.svg).
- [22] I. Horcas, R. Fernandez, JM Gomez-Rodriguez, J. Colchero, J. Gómez-Herrero, and AM Baro. WSxM: A software for scanning probe microscopy and a tool for nanotechnology. *Review of Scientific Instruments*, 78:013705, 2007.
- [23] Jaroslaw Drelich, Jan D. Miller, and Robert J. Good. The Effect of Drop (Bubble) Size on Advancing and Receding Contact Angles for Heterogeneous and Rough Solid Surfaces as Observed with Sessile-Drop and Captive-Bubble Techniques. *Journal of Colloid and Interface Science*, 179:37–50, October 1996.

- [24] Emanuele Ostuni, Robert G. Chapman, R. Erik Holmlin, Shuichi Takayama, and George M. Whitesides. A Survey of Structure - Property Relationships of Surfaces that Resist the Adsorption of Protein. *Langmuir*, 17:5605–5620, May 2001.
- [25] Masahide Taniguchi and Georges Belfort. Low protein fouling synthetic membranes by uv-assisted surface grafting modification: varying monomer type. *Journal of Membrane Science*, 231:147–157, November 2003.



## Appendix A

# Laboratory safety

*In this appendix the safety precautions which have to be taken with respect to chemicals and equipment are listed. The R- and S-phases of all chemicals have been listed, and furthermore issues with regard to the setup are presented.*

### **Glycidol**

- R21/22 Harmful in contact with skin and if swallowed
- R23 Toxic by inhalation
- R36/37/38 Irritating to eyes, respiratory system and skin
- R45 May cause cancer
- R60 May impair fertility
- R68 Possible risk of irreversible effects
- S26 In case of contact with eyes, rinse immediately with plenty of water and seek medical advice
- S36/37 Wear suitable protective clothing and gloves
- S45 In case of accident or if you feel unwell, seek medical advice immediately (show the label where possible)
- S53 Avoid exposure - obtain special instructions before use

### **Methanol**

- R11 Highly flammable

- R23/24/25 Toxic by inhalation, in contact with skin and if swallowed
- R39/23/24/25 Toxic: danger of very serious irreversible effects through inhalation, in contact with skin and if swallowed
- S7 Keep container tightly closed
- S16 Keep away from sources of ignition - No smoking
- S36/37 Wear suitable protective clothing and gloves
- S45 In case of accident or if you feel unwell, seek medical advice immediately (show the label where possible)

### **Sodium Methoxide**

- R11 Highly flammable
- R14 Reacts violently with water
- R34 Causes Burns
- S8 Keep container dry
- S16 Keep away from sources of ignition - no smoking
- S26 In case of contact with eyes, rinse immediately with plenty of water and seek medical advice
- S43 In case of fire, use sand, dry chemical or alcohol-resistant foam
- S45 In case of accident or if you feel unwell, seek medical advice immediately (Show the label where possible)

In order to overcome the hazards linked to the used chemicals, precautions were taken. Both in the polymerisation, the activation, and the deposition of waste it was incorporated that the substances were dangerous to handle, and a description of the concerns with respect to the method described in section 3.1.

During the activation, both methanol and sodium methoxide were used, making a variety of hazards present. Protection ware was used to keep the body from contact with the chemicals. Furthermore all handling were done in a fumehood, to prevent moisture to be inhaled. The glassware were rinsed with pure methanol and ethanol afterwards, all done in the fumehood, and transferred to Z-waste, the class containing waste which are not comparable with the other waste types.

In the polymerisation, glycidol was used. It was stored under ventilation and cooled between used, and transferred to the fumehood before opened. When the chemical were transferred to the reaction cell, precaution was taken to ensure no

spill from the flask. Again, protection ware was used to avoid exposure to the substance.

When the polymerisation was done, the glassware was rinsed with ethanol, and the waste transferred to C-waste. The glassware was cleaned with acid in order to oxidise the epoxides before new experiments.